Groundwater for Sustainable Development 11 (2020) 100467

Contents lists available at ScienceDirect

Groundwater for Sustainable Development

journal homepage: http://www.elsevier.com/locate/gsd

Research paper

Hydrogeochemical characterization and quality evaluation of groundwater suitability for domestic and agricultural uses in the state of Qatar

Ayesha Y. Ahmad [a], Mohammad A. Al-Ghouti [a,*], Majeda Khraisheh [b], Nabil Zouari [a]

[a] Department of Biological and Environmental Sciences, College of Arts and Sciences, Qatar University, P.O. Box 2713, Doha, Qatar
[b] Department of Chemical Engineering, College of Engineering, Qatar University, P.O. Box 2713, Doha, Qatar

ARTICLE INFO

Keywords:
Groundwater
Hydrogeochemical characterization
Domestic use
Agriculture use
Geochemical modeling
Geo-statistical analysis

ABSTRACT

This study aims to investigate the groundwater (GW) quality in Qatar to be utilized in domestic and agricultural uses. The integrated physiochemical analysis along with hydrochemical faces analysis, geochemical modeling, statistical and geostatistical analysis was conducted. The results showed that the GW samples mainly have the following cations $Na^+ > Ca^{2+} > Mg^{2+} > K^+$ abundantly, while $Cl^- > SO_4^{2-} > HCO_3^- > NO_3^-$ were the main anions. The obtained analytical values of the GW samples were plotted on Piper, Schoeller, Ternary, Ludwig Langelier, Giggenbach Triangle, Durov, and stiff graphs. The hydrogeochemical facies and the obtained graphs confirmed that most of the analyzed GW samples fall into two types of water namely calcium-chloride-type (SO_4–Cl and Ca–Mg) and sodium-chloride-type (SO_4–Cl and Na–K). Three principal components were yielded from the principal component analysis (PCA), which are the first principal component (PC1), second principal component (PC2), and third principal component (PC3) with ≥1 Eigenvalues, and total variance of 49, 31, and 19.9%, respectively. A positive loading of Mg, Th, Sr, Ca, TDS, SO4, Li, Cl, F, Br, Cd, K, Ba, and Na has been shown by the PC1; representing the factors which are contributing to the high salinity of the GW due to the salt water intrusion and the mineralization of rocks and soil which is supported by the water type classification and saturation indices. The PC2 showed a negative loading of U, Al, Se, Mo, Mg, and temperature, which could be associated with a localized sedimentary depositional or hydrogeochemical environment. The PC3 showed a positive loading of Ni, Zn, Be, pH, Cu, Co, Fe, B, V, and TOC, which indicates the dissolution and precipitation (reducing and oxidizing factor) such as iron which is a redox-sensitive variable.

1. Introduction

In arid regions, water resources management is a very complicated practice due to the limited water availability and accessibility, in addition to the climate change (Rajmohan et al., 2019). Groundwater (GW) is highly affected by both natural and anthropogenic activities, which might make it unsuitable for domestic and irrigated agriculture (Mallick et al., 2018). For example, sea level rise, saline water intrusion, high evaporation rates, and mineral weathering may increase the salinity and metals concentrations in the GW due to the dissolution of minerals under specific pH and redox levels (Alfy et al., 2017; Al-Shidi, 2014). The deterioration of GW quantity and quality is caused by the high demand for freshwater (Etteieb et al., 2015). Rapid urbanization, high agricultural development, and extensive GW pumping may affect GW quantity and quality (Al-Shidi, 2014). In addition, spills, sewage, and fertilizer leaching might influence the GW quality (Mallick et al., 2018).

The State of Qatar is located in the Arabian Gulf, which is considered as one of the semi-arid regions, with no surface water and restricted water resources from little rainfall; therefore, freshwater natural resources in Qatar are limited to GW (MDPS, 2015). Qatar has 80 mm average precipitation annually (MDPS, 2015). Desalination of seawater represents 59% of the total water production in Qatar, followed by a GW abstraction of about 30%, then treated wastewater that is used for agriculture and green spaces irrigation of about 11% (Baalousha, 2016). All the fresh GW in Qatar comes from local rainfall, except for the confined slightly brackish water in Abu Samara, which receives inflow GW from the west Saudi Arabia (UNDP, 2013). The annual recharge mainly comes from the infiltration of runoff, which is generally collected in surface depressions. The recharge of the GW by rainfall is estimated to be 25 million m^3 per year, which is similar to previous studies that estimated 7–10% of the annual rainfall (the average annual rainfall volume about 0.052 billion m^3) in the north of Qatar, and 3.5–5% in the

* Corresponding author.
E-mail addresses: mohammad.alghouti@qu.edu.qa, mohammad.alghouti@qu.edu.qa (M.A. Al-Ghouti).

https://doi.org/10.1016/j.gsd.2020.100467
Received 1 April 2020; Received in revised form 14 July 2020; Accepted 8 August 2020
Available online 14 August 2020

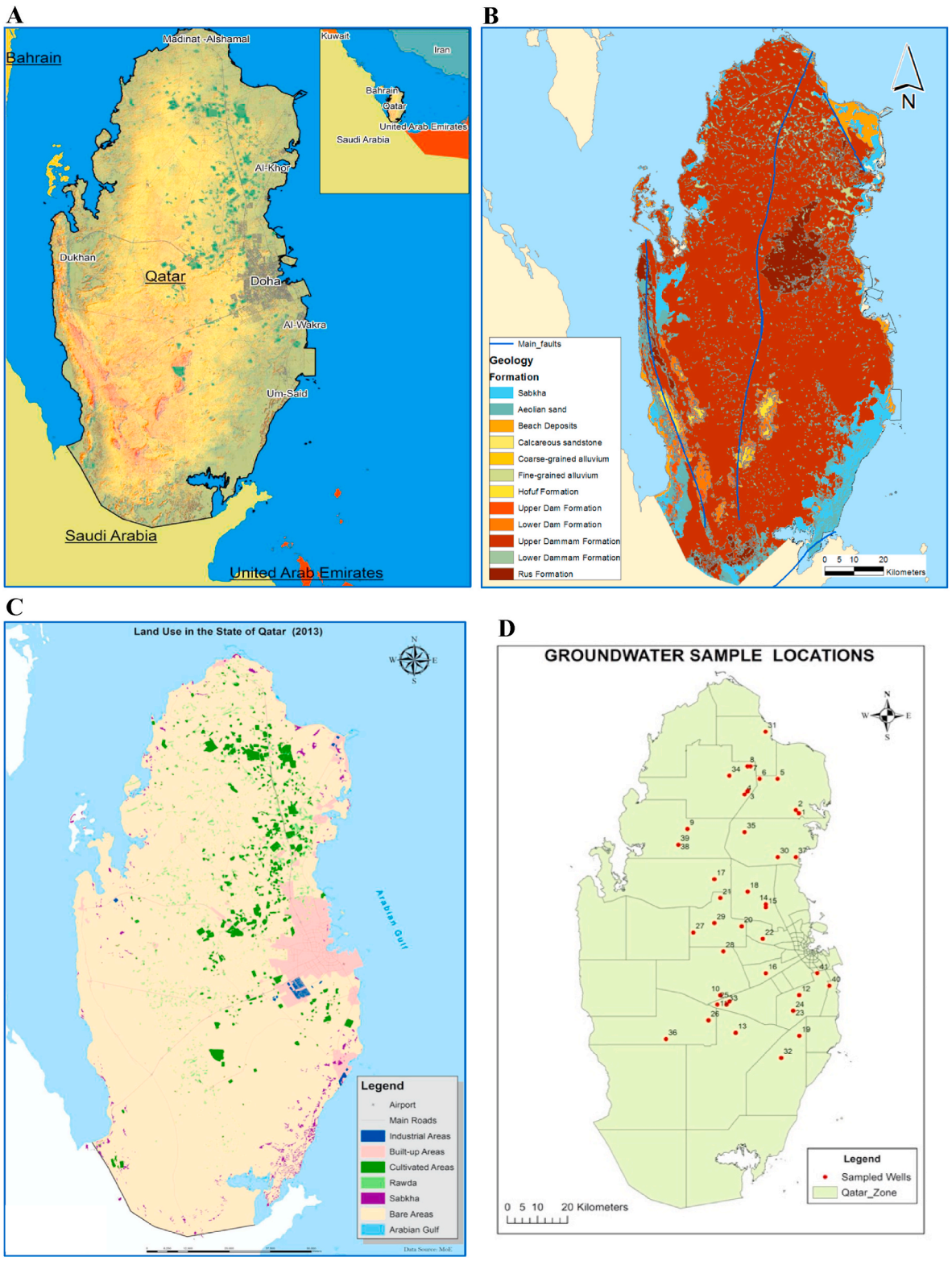

Fig. 1. A. Qatar Location map (Baalousha, 2016), B. Qatar geological map (Shomar et al., 2014), C. Qatar land use map (Shomar et al., 2014), and D. Groundwater Sample locations.

south of Qatar (Baalousha et al., 2015). However, the current GW abstraction reached 252.1 million m^3 per year, the annual water deficit due to the GW abstraction ranged from 100 million m^3 per year to 158 million m^3 per year during the period 2008–2014 (MDPS, 2015; SWS, 2009). The GW abstraction is mostly for agricultural uses accounting for 92% of total abstracted GW of about 230 million m^3 per year. In 2014, no GW wells were characterized as non-saline or slightly saline, while 60% of GW wells were moderately saline and 40% highly saline (MDPS, 2015). Current GW abstraction greatly exceeds the rate of rainfall-induced recharge and this continues to result in the GW levels declining (MDPS, 2015). About 70% of the abstraction was from the north basin, such that the wells drill the Rus formation, which is of a

depth 60–70 m. The overall number of wells with various uses was greater than 8509 where 74% of the overall wells are farm wells of about 6299 wells (SWS, 2009). The GW basins in Qatar were classified into north, south, Abou-Samra, and Doha GW basins (SWS, 2009). The vast majority of wells are in the north and south GW basins, the north and south GW basins make up about 70% and 28% of total wells in Qatar, respectively (SWS, 2009). The over-extraction of Qatar's GW aquifers can reduce the aquifer levels, causing the seawater intrusion; thus, the GW is highly vulnerable to salinization (Kuiper et al., 2015).

Climate change such as the decrease in precipitation and increase in evapotranspiration has a destructive result on the GW level due to the decrease in the GW recharge (Hoyos et al., 2016). For example, high evaporation of shallow GW may cause the dissolution of mostly halite and gypsum (Shomar, 2015). Among other climate processes, sand/dust storms and soil erosion may cause significant changes in the topsoil geochemistry (Shomar, 2015). Salinization of GW is a significant environmental issue. GW salinization mainly occurs as a result of high GW extraction which introduces the saline water from the deep underlying basement rock, from deep-buried valleys or from adjacent surface water bodies, which also could be aggravated by drought and sea-level rise (Suursoo et al., 2017). The GW salinization might increase the total dissolved solids and enhance water-rock interaction (Vinson et al., 2013). A strong relationship between elevated levels of naturally occurring element levels such as the trace elements and minerals present in soils and rocks with salinity, as the hydrogeochemical condition has an important function in the distribution of these natural elements in the GW (Walsh et al., 2014). Soil with high salinity and metals mobility are significantly correlated, and this could increase the metal levels in GW (Shomar, 2015). The water resources are globally threatened by different contaminants (Manickum et al., 2014). For example, fertilizers, pesticides, and sewage can be an anthropogenic source of toxic elements in GW (Seyedmohammadi et al., 2016). The produced water or coproduced water from oil and gas industries is very salty and contains a mixture of organic and inorganic residues; and generally, this produced water is disposed of with or without treatment to the sea or into the deep aquifer (Shomar, 2015). According to Shomar (2015) and Smedley and Kinniburgh (2017), the physicochemical characterization of the produced water and aquifer determine the different severe reactions and environmental consequences that might happen.

In a study, investigating the physicochemical characteristics of carboniferous aquifers demonstrated that hydrogeochemical changes are induced by not only natural but also anthropogenic processes (Galitskaya et al., 2013). The prime reason for hydrogeochemical changes is the disturbing of the hydrodynamic regime, such as the exploitation of the GW (Galitskaya et al., 2013). The local hydrogeological formations must be considered when allowing the maximum production rates as well as for developing a water quality-monitoring plan (Suursoo et al., 2017). The GW quality is also affected by rock interaction within the aquifer and the soil above the aquifer. Shallow coastal aquifers are more vulnerable to be contaminated from surface soil due to the relatively short distance needed to reach the water table (Shomar, 2015; Kuiper et al., 2015). Carbonate aquifers in Qatar are within the karst formation and depressions; generally, karst aquifers are susceptible to pollution (Sadiq and Nasir, 2002). Anthropogenic contamination from agricultural effluents, and wastewater, above very fractures strata, could infiltrate contaminant very fast into the aquifer and extend over a large area (Baalousha, 2016). This is crucial, especially with the high economic growth, and the population of Qatar increase from 600,000 in 2000 to 2,685,000 in 2018 (MDPS, 2018). In Qatar, shallow GW with high hydraulic conductivity in the coastal and northern aquifers are of a high vulnerability because of the depression areas, consequently, the southwest aquifers showed low vulnerability because of thick formations and vadose zone with a clay layer (midra shale), that block infiltration of water (Baalousha, 2016). In summary, the quality of GW can be affected by natural and anthropogenic variables such as climate change, drought, overexploitation, and socioeconomic development. Thus, assessing the GW resource in arid countries such as Qatar is of high importance due to its critical economic and social values as there are no other renewable water resources (Abdel-Satar et al., 2017).

Sustainable management of water resources relies on an integrated assessment of the hydrogeochemical systems (Khan et al., 2019). Various combined hydrochemical processes determine the quality of GW along with its flow path such as biological processes, weathering, ion exchange, and dissolution. The dissolution generally happens in the recharge zones and ion exchange happens along the flow path. On the other hand, ion exchange, evaporation, and precipitation takes place mainly in the discharge zones (Mallick et al., 2018). Thus, the formation of the hydrochemical facies/water types is a result of the geochemistry of the GW, which is further controlled by the geological structure and mineralogy of the aquifer (Ravikumar and Somashekar, 2015).

Different methodologies have been used to study the hydrogeochemical process and to investigate the quality of the GW such as multivariate statistical analysis, geochemical modeling, and using stable isotopes (Mallick et al., 2018). The current study evaluates the quality of the GW and related hydrogeochemical processes using up to date hydrochemical graphical methods, geostatistical, and statistical analysis. Further, the study demonstrated the effects of agricultural practices in view of the natural influences (geological, hydrogeological, and climatic) and the anthropogenic influences (agricultural) to support farmers, decision-makers, stakeholders to achieve sustainable GW management.

2. Materials and methods

2.1. Study area

Qatar is located on the Arabian Peninsula, in the eastern region as shown in Fig. 1A. Qatar has 11,586 km^2 total surface area, it is about 180 km in length and 90 km in width (Baalousha, 2016). Qatar is an arid country and has flat rocky surfaces. Nevertheless, it consists of some hills of 100 m above sea level. The northern region of Qatar is relatively little elevations that are higher in the west and southwest, it is about 6 m below the sea level in Dukhan Sabkha to about 103 m above the sea level in the southwest. Qatar is mostly located over a uniform limestone bed. The oldest exposed rocks are the Lower Eocene Rus Formation, which mostly contains dolomite and limestone with some dispersed rocks of Miocene (covering about 8%) of the surface area (MDPS, 2015). Karst is extensive in Qatar, it involves depressions, sinkholes, caves, and solution hollows. It is associated with the calcareous, dolomitic, and gypsiferous, anhydrite horizons of the Eocene Rus and Dammam formations. It happened because of preferential dissolution related to the variation in composition between dolomite, calcite, and gypsum rocks (Sadiq and Nasir, 2002).

Potable water has been found in Eocene age rocks in Qatar while the brackish GW has been found in upper Cretaceous age rocks (Shamrukh, 2012). In Qatar, the descriptions of the Middle Eocene age are Dammam formation, Rus formation, while Umm er-Radhuma is the Early Eocene/Paleocene age as shown in Fig. 1B (Shomar et al., 2014; Al-Naimi and Mgbeojedo, 2018). The Dammam formation appears over most of the Qatar peninsula, the depth of the formation is about 50 m. The upper part has limestone, called the Abarug Member, underlain by chalky limestone, called the Umm Bab member and the lower part has a massive clayey fossiliferous limestone, known as the Dukhan member, underlain by the Midra Shale member of low carbonate (Al-Saad, 2005). The upper part is significantly fractured and has solution cavities (Alsharhan et al., 2001). The Rus formation conformably lies under the Dammam formation. The depth of Rus formation varies from 28 to 44 m in the north and central of Qatar, and about 110 m in the south-west of Qatar (Al-Yousef, 2003). It contains an abundance of limestone, dolomite, anhydrite, and some marl (UNDP, 2013). Umm er-Radhuma formation conformably lies under the Rus. It comprises a dense sequence of

about 300–500 m of brownish or grayish limestone that is dolomitic and well porous in the upper part which characterized by the presence of well-fractured karstic dolomite (Mohammad and Francois, 2019). Most wells in the center and south of Qatar reportedly tap the Rus formation aquifer, above the confining gypsum that covers up the Umm er-Radhuma formation aquifer. In north Qatar, most wells reportedly tap both the Rus and the upper of Umm er-Radhuma formation aquifer. While in the Abo Samra (southwest) GW wells reportedly tap the Alat aquifer of the Dammam formation, and some tap deep older Aruma aquifer of Aruma formation, which comes from Saudi Arabia (Al-Yousef, 2003). Aquifers of Dammam formation is unconfined in many areas due to erosion of the confining layers and/or the formation of karst structures (Alsharhan et al., 2001). The land use map in Fig. 1C shows that most of the agriculture activities are in the north of Qatar due to the larger size (19% of Qatar surface area) and less salinity levels (500–3000 mg Cl/L) of northern aquifer than southern aquifer (>5000 mg Cl/L) (Shomar et al., 2014).

2.2. Samples collection

The GW samples were collected from 41 locations throughout Qatar directly after the rainy winter season in May 2019, which reflects the groundwater salinity and good data for summer season comparison for future studies. The sampling wells were randomly selected from private farms with existing operation pumping wells where water discharge could be accessed. The sample locations are shown in Fig. 1D. To give a good spatial coverage over the entire studied area (farm wells), the sampling wells covered the north and south GW basins. However, the number of north wells is more than the number of the south wells because the north wells are less saline than south wells due to the karst formations in the north that allow rainwater penetration to the aquifer (Sadiq and Nasir, 2002). The sampling procedures were carried out based on ISO 5667–11:2009, 2009 to guarantee that the samples are representative of the GW conditions underneath the investigation location and not stagnant water within the wells, thus the water is pumped for an adequate time (at least 30 min). The samples were collected directly from the faucet at the wellhead such that the sample comes freshly from deep in the well.

The sample bottles were pre-cleaned with nitric acid and each sample was acidified by 1 mL nitric acid (50%) pH < 2 for the cation, trace elements, and toxic metals analysis, while for the anion analysis they were not acidified. The sample bottles were rinsed 3–4 times with water from the well and then duplicated polyethylene bottles of 1-L size were filled completely to prevent degassing. Triplicated topsoil samples of 1 kg size are taken into polyethylene bags from three different locations around the well about 1–10 m. The samples were shoveled by a corer drill of 30 cm × 30 cm with approximately depth of 10 cm. Any observation, which may affect the results of the analysis, for instance, the production of bubbles, smell, color, and sediment were highlighted and recorded. Any possible sources of contamination in the vicinity of the well site, for instance, oil spills, fertilizers, pesticides, or landfills were also recorded in the field datasheets. The sample bottles were kept securely in a cooler box containing ice until delivered to the laboratory and kept at 4 °C.

2.3. Field analyses

Various parameters were measured immediately on site, such as temperature, pH, total dissolved solids (TDS), and electrical conductivity (EC) by a portable pH, conductivity, salinity, and temperature multimeter (Handheld YSI Model 63). The multimeter was calibrated before each field measurement using standard solutions, pH buffer (citric acid and disodium hydrogen phosphate, also known as a citrate-phosphate buffer), and the EC buffer KCl (potassium chloride), and the multimeter electrode was rinsed with distilled water before measurements.

2.4. Physiochemical characteristics analysis

The pH value was measured again along with the EC in the lab using the multimeter (Handheld YSI Model 63). Electrical conductivity ($\mu S/cm$) at 25 °C was used to determine the TDS value in (mg/L). The relationships of TDS and specific electrical conductivity (SEC) of the GW were calculated based on equations (1) and (2):

$$\mathrm{TDS} = \mathrm{SEC} \times 0.65 (\text{for SEC} < 5000 \mu S/cm) \quad (1)$$

$$\mathrm{TDS} = \mathrm{SEC} \times 0.70 (\text{for SEC} > 5000 \mu S/cm) \quad (2)$$

The factors of 0.70 for greater than 5000 μS/cm and 0.65 for less than 5000 μS/cm were determined from the historical data and verified during the Schlumberger Water Services study in Qatar with a correlation coefficient of 0.99. The total water hardness was calculated using equation (3) as determined by (Al-Shidi, 2014).

$$\text{Total Water hardness}(\mathrm{mg/L\ of\ CaCo_3}) = \mathrm{Ca(mg/L)} \times 2.497 + \mathrm{Mg(mg/L)} \times 4.118 \quad (3)$$

For the main cations and anions, namely chloride, sulfate, calcium, magnesium, sodium, potassium, fluoride, and nitrate were analyzed using an ion chromatography device (850 Professional IC Detector). The trace element and toxic metals analysis were analyzed using inductively coupled plasma mass spectrometry (ICP-MS) PerkinElmer, model NexION 300 D. The soil samples were prepared by acid digestion with HNO_3 and HF in a hot block apparatus. The prepared samples were analyzed for inorganic chemicals using ICP-MS.

2.5. Statistical analysis

The statistical package for the social sciences (SPSS) was employed to statistically analyze the data. Descriptive statistics were computed such as the minimum, maximum, mean, median, and standard deviation values. Regression analysis (r) and Pearson's correlation coefficients were also calculated between the quality parameters of the GW samples. The correlation coefficients between the quality parameters pairs of the GW and the soil samples were also computed. The GW quality parameters were examined for significant differences between different locations by the *t*-test and ANOVA test. PCA is computed to recognize the pattern of the analyzed variables. Unscrambler X (v10.5, Camo Analytics—USA) following singular value decomposition (SVD) algorithm and XLSTAT 2016 (MS Excel, 2016; Microsoft–USA) was used for the PCA and clustering of variables.

2.6. Geostatistical analysis

The spatial analysis tool of ArcGIS 10.3.3 software was used to analyze the spatial variation of the GW quality parameters. The inverse distance weighted (IDW) and simple Kriging algorithms were used to interpolate the point data at unmeasured locations and generate the surface map. The IDW method was modeled using best-fitted power; while Kriging was used the best-fitted semi-variograms. Cross-validations were computed with trend data to select the lowest root mean square error in the IDW; while Kriging selected the lowest error by comparing the sampled and the predicted values through employing the empirical semi-variogram models.

2.7. Hydrogeochemical water quality analysis

AquaChem software is widely used to analyze, plot, and report aqueous geochemistry and water quality of the GW supply wells. Major ions relative levels of the studied GW samples were plotted using AquaChem version 4.0.264 from Waterloo Hydrogeologic, 2003). General water quality diagrams were generated such as Piper, Schoeller,

Table 1
Summary of the statistical analysis of the physicochemical characteristics of the GW samples.

	N	Range	Minimum	Maximum	Mean		Std. Deviation	Variance	Skewness		Kurtosis	
	Statistic	Statistic	Statistic	Statistic	Statistic	Std. Error	Statistic	Statistic	Statistic	Std. Error	Statistic	Std. Error
pH	41	1.05	6.89	7.94	7.30	0.037	0.238	0.057	0.795	0.369	0.714	0.724
Conductivity (μS/cm)	41	21.41	0.92	22.33	7.29	0.739	4.734	22.41	1.449	0.369	2.384	0.724
TDS (mg/L)	41	15034	598.87	15633	5038.1	525.93	3367.7	11341125	1.408	0.369	2.211	0.724
TOC (mg/L)	41	34.23	1.27	35.50	14.62	1.20	7.726	59.695	0.370	0.369	−0.104	0.724
SAR	41	31.72	1.55	33.27	12.781	1.30	8.383	70.291	1.054	0.369	0.310	0.724
Hardness	41	5117.9	275.16	5393.0	2120.2	163.88	1049.3	1101123	0.762	0.369	1.350	0.724
Potassium (mg/L)	41	304.3	16.36	320.7	90.18	8.880	56.86	3234	2.231	0.369	6.610	0.724
Magnesium (mg/L)	41	395.8	24.41	420.2	169.1	14.85	95.09	9043	0.731	0.369	0.275	0.724
Calcium (mg/L)	41	1428	69.94	1498	570.2	43.28	277.1	76808	0.784	0.369	1.994	0.724
Sodium (mg/L)	41	5483	64.23	5547	1466	194.3	1244	1547199	1.438	0.369	1.899	0.724
Chloride (mg/L)	41	30603	203.68	30807	6289.5	1053.8	6747.5	45528899	2.100	0.369	4.865	0.724
Fluoride (mg/L)	41	7.18	1.59	8.77	3.81	0.246	1.58	2.48	0.974	0.369	1.049	0.724
Bromide (mg/L)	41	21.61	0.37	21.98	4.32	0.758	4.85	23.56	2.547	0.369	6.576	0.724
Nitrate (mg/L)	41	113.3	0.00	113.3	36.32	4.309	27.59	761.3	1.207	0.369	1.116	0.724
Sulfate (mg/L)	41	11543	53.46	11596	4977.2	389.06	2491.2	6205964	0.042	0.369	−0.004	0.724
Lithium (μg/L)	41	213.4	23.34	236.7	120.6	8.705	55.74	3107	0.488	0.369	−0.605	0.724
Boron (μg/L)	41	3431	388.0	3819	1885	118.0	755.8	571195	0.225	0.369	0.066	0.724
Molybdenum (μg/L)	41	286.1	7.830	294.0	53.88	7.042	45.10	2033	3.927	0.369	20.29	0.724
Selenium (μg/L)	41	20.55	1.540	22.09	8.882	0.773	4.95	24.52	0.680	0.369	−0.283	0.724
Strontium (μg/L)	41	16740	3534	20273	13226	720.59	4614.1	21289539	−0.294	0.369	−0.925	0.724
Chromium (μg/L)	41	11.79	0.100	11.89	3.912	0.534	3.419	11.69	0.782	0.369	−0.699	0.724
Uranium (μg/L)	41	31.13	0.110	31.24	1.630	0.746	4.770	22.82	6.248	0.369	39.63	0.724
Vanadium (μg/L)	41	35.50	1.490	36.99	14.36	1.015	6.500	42.26	0.603	0.369	2.701	0.724
Manganese (μg/L)	41	4.980	0.010	4.99	1.009	0.216	1.38	1.92	1.862	0.369	2.786	0.724
Iron (μg/L)	38	118	0.01	118	4.72	3.07	18.91	357.8	6.119	0.383	37.62	0.750
Nickel (μg/L)	41	11.38	0.24	11.62	1.94	.305	1.95	3.83	3.450	0.369	14.91	0.724
Cobalt (μg/L)	41	0.45	0.01	0.46	0.0712	.0136	0.08	0.008	3.481	0.369	12.87	0.724
Copper (μg/L)	41	4.36	0.08	4.44	1.37	0.154	0.99	0.982	1.022	0.369	0.911	0.724
Aluminum (μg/L)	13	7.46	0.15	7.61	1.50	0.577	2.08	4.33	2.487	0.616	6.521	1.191
Beryllium (μg/L)	19	0.14	0.00	0.14	0.081	0.009	0.04	0.002	0.169	0.524	−0.868	1.014
Zinc (μg/L)	20	51.25	0.03	51.28	5.88	2.51	11.23	126.25	3.820	0.512	15.76	0.992
Arsenic (μg/L)	41	4.39	0.61	5.00	2.00	0.153	0.98	0.971	0.770	0.369	0.622	0.724
Cadmium (μg/L)	31	0.49	0.00	0.49	.0723	0.016	0.091	0.008	3.474	0.421	14.97	0.821
Barium (μg/L)	41	21.55	3.07	24.62	10.20	0.671	4.30	18.497	1.239	0.369	2.076	0.724

Ternary, Ludwig Langelier, Giggenbach Triangle, Durov, stiff plots, and Wilcox Plot for irrigation hazard Stiff plots. The saturation index (SI) and aqueous mineral phases were calculated using the inverse geochemical modeling along with the thermodynamic program PHREEQC. The changes in saturation state were used to identify the geochemical reactions governing the GW chemistry such that the negative values of SI; suggesting that the GW was undersaturated, while the positive values indicate oversaturation of the GW with respective minerals. Saturation index (SI) is defined by Mallick et al. (2018) as illustrated in equation (4),

$$SI = \log (IAP/Ksp) \quad (4)$$

where IAP is the ion activity production and Ksp is the equilibrium solubility product.

3. Results and discussion

3.1. Physical and chemical properties of the collected GW samples

The physicochemical characterizations of the collected GW samples are summarized in Table 1. The temperatures ranged from 17.3 °C to 31.7 °C with an average of 27.7 °C. The variations of the sample temperature were due to the GW recharge with rainfall, that deep GW has a relatively higher temperature than shallow GW. The measurement of the GW pH gives significant information about the geochemical equilibrium (Mallick et al., 2018). An interpolated map (Fig. 2A) shows the pH value variation in the study locations. The pH values varied from 6.8 to 7.9 with an average of 7.3, which is within the world health organization (WHO) standard of (6.5–8.5) (WHO, 2017). An exception from two slightly acidic wells (pH = 6.9 and 6.8), which are due to the use of the fertilizer in the farms near the wells. The result of pH showed the alkalinity of the aquifers due to the interaction between soil and water such as the dissolution of limestone and the equilibrium of calcite dissociation as follows:

$$CaCO_3 + H_2O \; Ca^{2+} + HCO_3^- + OH^- \quad (5)$$

Under normal conditions, the alkaline GW does not show high levels of toxic metals (Shomar, 2015).

The total hardness varied from 275 to 5393 mg $CaCO_3$/L with an average of 2120 mg $CaCO_3$/L. An interpolated map (Fig. 2B) shows the total hardness variations in the study area. Alsuhaimi et al. (2019) stated the degrees of hardness as soft (0–75 mg $CaCO_3$/L), moderate (75–150 mg $CaCO_3$/L), hard (150–300 mg $CaCO_3$/L), very hard (>300 mg $CaCO_3$/L). According to this classification, the total hardness of the GW is classified as very hard except for one sample, which was hard. The results showed the limitation to use the GW in industrial and irrigation pipes because water should have a total hardness of less than 85 mg $CaCO_3$/L and magnesium hardness of less than 40 mg $CaCO_3$/L to minimize scaling at elevated temperatures (Al-Shidi, 2014). Srinivasamoorthy et al. (2014) indicated that the presence of calcium carbonate ($CaCO_3$) in GW leads to temporary hardness in which heat can be used to reduce it. However, Ca^{2+} and Mg^{2+} ions cause the permanent hardness where ion-exchange processes can be utilized to reduce the ions. The salinity of GW can be evaluated by testing its EC. Total dissolved solids (TDS) are the sum of all dissolved inorganic salts in the water such as carbonate, bicarbonate, chloride, fluoride, sulfate, phosphate, nitrate, calcium, magnesium, sodium, and potassium (Adimalla and

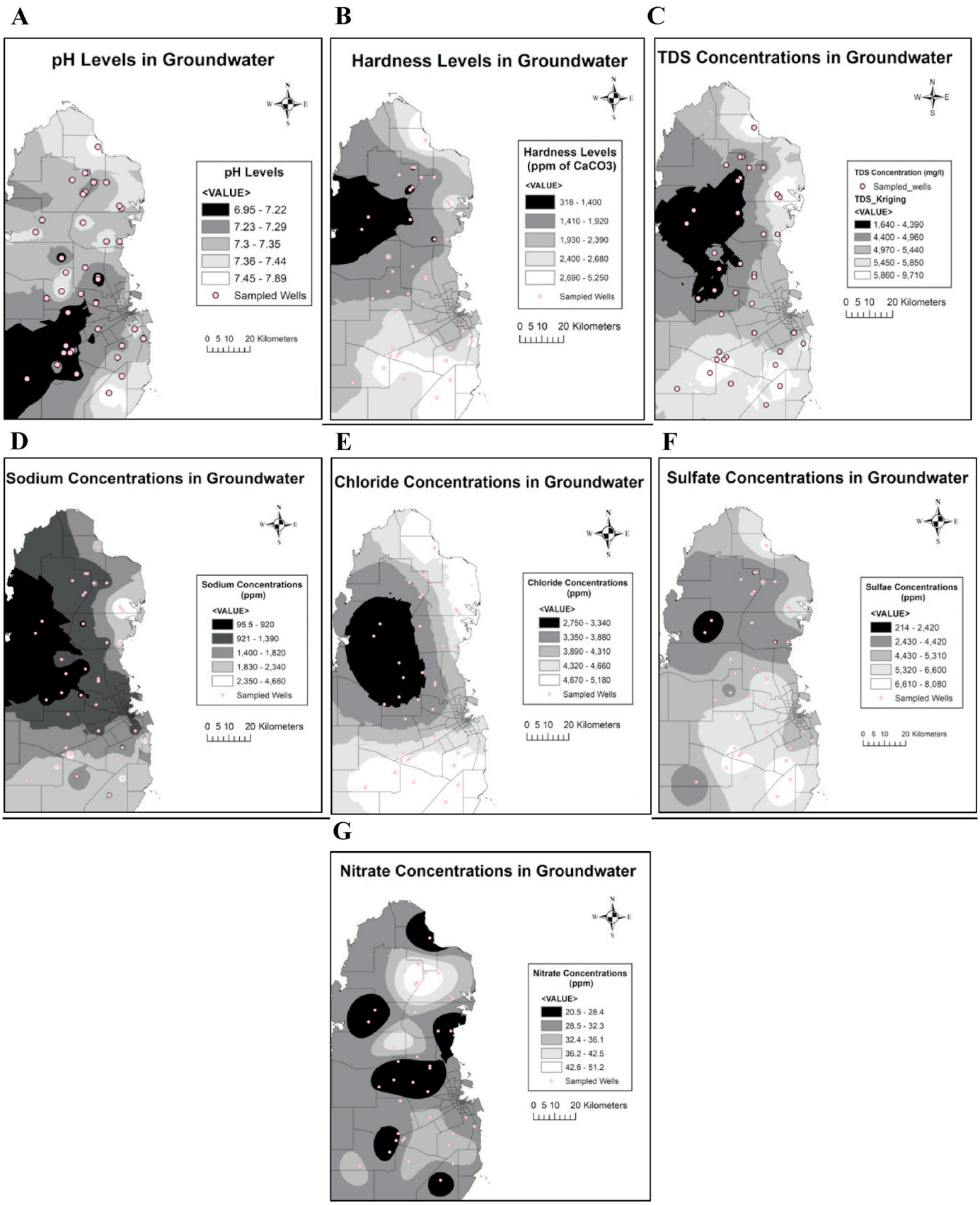

Fig. 2. Distribution Maps of **A**. pH, **B**. hardness, **C**. TDS, **D**. Sodium, **E**. Chloride, **F**. Sulfate, **G**. Nitrate.

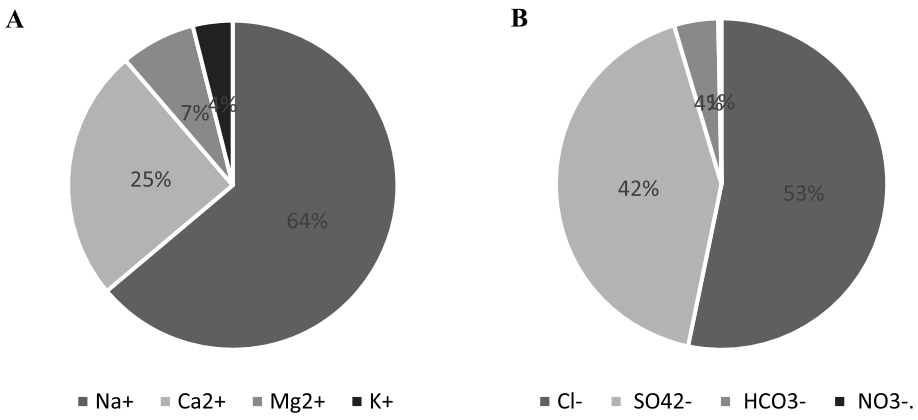

Fig. 3. Distribution of **A**. major cations and **B**. major anions in the GW of the study area.

Venkatayogi, 2018). An interpolated map (Fig. 2C) shows the TDS variations in the study area. In the current study, the range of the electrical conductivity (EC) was (0.92–22.33 μS/cm), and the average of EC was 7.29 μS/cm. The range of TDS was (598–15633 mg/L) and the average TDS was 5038 mg/L. Ghalib (2017) stated that the classification of EC as low saline (EC = 1500 μS/cm), medium saline (EC between 1500 and 3000 μS/cm) and high saline (EC > 3000 μS/cm). According to this classification, there were no samples where having EC less than 500 μS/cm that can be considered similar to freshwater. Only two samples were low salinity of less than 1500 μS/cm. Only one sample was moderately saline of the EC, which was between 1500 and 3000 μS/cm 38 samples were highly saline of the EC, which were greater than 1500 μS/cm, and do not meet the limits of drinking water (WHO, 2017). While 38 were highly saline with EC greater than 3000 μS/cm, which is unsuitable for water irrigation (Misstear et al., 2017). The weather, the host rock, and the residence time of the GW in the aquifer are the main factors that change TDS values (Alsuhaimi et al., 2019). Thus, in this study, the high EC (high salinity) in the GW is due to the aridity of Qatar with low precipitation and high evaporation. Furthermore, agricultural activities such as using fertilizers and keep irrigation using high saline GW may lead to concentrating salts in the soil due to high evaporation, which may leach of salts and nutrients to the aquifer. Heavy extraction of the GW leads to the migration of the brackish water from the deep aquifer or adjacent seawater. High TDS levels were detected along the coastal areas as shown in the interpolation map, which might be attributed to the seawater intrusion that will lead to increase EC, whereas high values in southern areas might be attributed to lower rainfall and deep water (brackish) mixing. However, GW consists of several chemicals that are found at various levels. Generally, 95% of the ions found in the GW are Na^+, K^+, Ca^{2+}, Mg^{2+}, Cl^-, SO_4^{2-}, HCO_3^-, and NO_3^- (Sundaram et al., 2009). The main source of ions in GW is the lithology of rocks in contrast with anthropogenic sources (Abdel-Satar et al., 2017).

3.1.1. Major anions analysis

As shown in Fig. 3B, major anions in the study area were found to be in the following order $Cl^- > SO_4^{2-} > HCO_3^- > NO_3^-$. Cl^- was found as the most dominant anion among other tested anions with values between 203.6 and 30806 mg/L with a mean value of 6289 mg/L, followed by SO_4^{2-} ranging from 53.4 to 11596 mg/L with a mean value of 4977 mg/L. HCO_3^- values were between 282.3 and 975.6 mg/L with a mean value of 509.1 mg/L. NO_3^- values were in the range of 5.2 and 113.3 mg/L with 37.2 mg/L as a mean value.

Chlorides were common constituents in natural water. Natural sources of Cl− in the GW include rainwater, rock-water interactions, saline seeps, while anthropogenic sources are fertilizers such as gypsum fertilizers (Vengosh et al., 2002), road salt, industrial facilities' effluents, sewage water pollutants, and municipal landfills' leachate (Srinivasamoorthy et al., 2014). In the study area, the Cl^- sources are sewage water pollution, treated wastewater, rock water interaction, and seawater intrusion. Laxative effects and salty tastes in drinking water can be caused by the elevated concentrations of Cl^- (Adimalla and Venkatayogi, 2018). Cl^- and Na^+ levels are correlated to the TDS and major ions in the samples. Fig. 2D and E clearly illustrate the variations of Na^+ and Cl^-, respectively.

When the sulfide minerals interact with water, they release SO_4^{2-} from the oxidation process. The igneous and sedimentary rocks such as gypsum ($CaSO_4{\cdot}2H_2O$) and anhydrite ($CaSO_4$) are a source of metallic sulfate (Czerewko et al., 2003). The map of sulfate ion (SO_4^{2-}) distribution (Fig. 2F) shows that the highest values are in the southern regions that might be related to sulfate ion dissolution along the flow path, and fertilizers and agriculture wastes leachate from the intensive agriculture activities in the study area. Furthermore, it can be attributed to gypsum and anhydrite dissolution within the limestone sequence. Anthropogenic sources such as industrial activities are attributed to high sulfate in the GW (El Maghraby et al., 2013). Thus, high SO_4^{2-} in some samples are due to natural sources such as gypsum rock dissolution and anthropogenic sources such as fertilizers from agriculture activities. Water with high Cl^- and SO_4^{2-} can cause hypertension, osteoporosis, stroke, laxative effect, diarrhea, asthma, dehydration, and gastrointestinal irritation and affect human health. SO_4^{2-} induces metals corrosion in the distribution system with low alkalinity water (Ghalib, 2017).

The concentration of bicarbonate and carbonate in the GW may be attributed to the carbonate weathering such as weathering of silicates. When feldspar minerals react with carbonic acid in water, it causes carbonic acid dissolution (Kumar et al., 2009). High HCO^- levels in the GW indicate the dominance of mineral dissolution (Ghalib, 2017). According to (SWS, 2009), wells categorized according to the hydrological basins in which they are found. The hydrological basins are based on the surface water run-off in Qatar and the average well depth by hydrological basin was measured as shown in the statistical analysis section. In this study, the levels of sulfate and chloride show an indirect relationship with the depth of GW table, while the level of HCO_3^- shows a direct relationship with the depth of GW table that HCO_3^- might indicate the formation of clay or limestone/dolomite presence in the area. All the parameters, except HCO_3, increase from inland to coast. It is also noticed that high EC is related to low bicarbonate levels.

Nitrate (NO_3^-) is found naturally in soil by biological oxidation of nitrogenous substances and it is an important plant nutrient. The presence of NO_3^- in the GW is from the use of fertilizers, sewage leaching, and agricultural/municipal waste (Mallick et al., 2018). Agriculture activities and organic nitrogen fertilizer from animal manures, human wastes, and sewage sludge, and inorganic nitrogen fertilizers contain NO_3^- and/or NH_4^+ (Rajmohan et al., 2019). In the current study, the high levels of NO_3^- could be attributed to the use of fertilizers. NO_3^- source in the GW is related to the infiltrated water quality, type of the soil, and

Table 2
Summary of the statistical analysis of the main trace elements in the soil samples.

	N	Range	Minimum	Maximum	Mean	Std. Deviation	Variance
	Statistic	Statistic	Statistic	Statistic	Statistic	Statistic	Statistic
Potassium (mg/g)	41	11.85	7.180	19.03	13.10	2.800	7873
Sodium (mg/g)	41	40.66	11.15	51.81	25.56	9.620	92582
Lithium (μg/g)	41	22.03	9.060	31.09	16.27	5.790	33.58
Boron (mg/g)	41	14.88	1.130	16.02	4.900	2.850	8152
Selenium (μg/g)	41	5.94	0.030	5.970	2.620	1.680	2.830
Strontium (μg/g)	41	5.57	0.492	6.069	1.631	1.131	1280
Chromium (μg/g)	41	552.7	28.68	3589	193.9	3560	305507
Manganese (μg/g)	41	750.1	168.7	918.8	408.2	151.2	22874
Iron (mg/g)	38	33.65	6.450	40.11	15.51	7.650	58644
Cobalt (μg/g)	41	19.47	3.190	22.66	7.420	4.610	21.32
Copper (μg/g)	41	38.84	12.15	51.00	25.68	9.720	94.59
Arsenic (μg/g)	41	13.22	0.230	13.45	5.500	3.080	9.530
Cadmium (μg/g)	41	0.437	0.020	0.457	0.167	0.108	0.012
Barium (μg/g)	41	294.5	213.0	507.6	355.4	60.07	3609

leaching process. Drinking water with a high NO_3^- level causes infants to have methemoglobinemia. Furthermore, it causes cyanosis, oral, colon, gastrointestinal, and lymphoma cancers, (Adimalla and Venkatayogi, 2018; Al-Kalbani and Price, 2015). NO_3^- in the GW had an average concentration of 36.32 mg/L. As illustrated in Fig. 2G, the central and northern regions of the study area had the highest NO_3^- values. High NO_3^- in the current study might be ascribed to agriculture activities such as manure use, especially at the shallow GW locations (Shomar, 2015).

The fluoride in the GW ranged from 1.5 to 8.7 mg/L, and the average value was 3.8 mg/L. Fluoride concentrations in all samples were higher than the drinking permissible limits (>1.5 mg/L). The sources of fluoride in the GW are the erosion of natural deposits such as granite, granite gneisses, and pegmatite (Adimalla and Venkatayogi, 2018; Alsuhaimi et al., 2019). Fluorosis that fluoride related to the teeth and bones health can be caused by high fluoride levels in drinking water (Rajmohan et al., 2019).

3.1.2. Major cations analysis

As illustrated in Fig. 3A, the major cations had the following order $Na^+ > Ca^{2+} > Mg^{2+} > K^+$. The results showed that Na^+ was mostly dominant among other cations with values varying from 64.2 to 5547 mg/L with a mean of 1466 mg/L, followed by Ca^{2+} ranging from 69.9 to 1497 mg/L with a mean value of 570.1 mg/L. Mg^{2+} values were in the range of 24.4–420.1 mg/L with a mean of 169.1 mg/L, while K^+ values ranged from 16.3 to 320.6 mg/L with a mean of 90.1 mg/L.

Sodium has high water solubility. High levels of Na^+ in the GW occur naturally in some regions from weathering rock-forming minerals such as halite, plagioclase feldspar mineral and argillaceous sediments. However, high sodium in the GW above natural levels may be related to anthropogenic sources like sewage effluent and leaching from landfills, industrial, road salt, and animal waste sites or saltwater intrusion (Ghalib, 2017). Various serious health issues can be induced by Na^+ levels above 200 mg/L, including nervous and kidney disorders, congenital diseases, and hypertension, in addition to circulatory and cardiac problems in the human body (WHO, 2017). In the current study, only two samples were Na^+ less than 200 mg/L, which may be related to the GW recharge events, leading to the dilution by infiltrated water. Thirty-nine samples were unsuitable for drinking due to the significant Na^+ level ($Na^+ > 200$ mg/L).

Forty samples were above the drinking water guidelines of Ca^{2+} of 75 mg/L (highest desirable limit (HDL) and thirty-eight samples were higher than 200 mg/L, which is the maximum allowable limit (MAL) recommended by (WHO, 2017). Mg^{2+} levels were unsuitable for drinking as shown in Table 1. High calcium levels in drinking water cause health issues such as kidney or bladder stones (WHO, 2017). The source of calcium in the GW is the dissolution of carbonates from sedimentary rocks and evaporitic minerals such as limestone or dolomite, calcite, dolomite, aragonite, and the most abundant among others in the study area, gypsum and anhydrite. Furthermore, weathering processes of silicate minerals can lead to the formation of calcium (Alsuhaimi et al., 2019). Also, increased concentrations of Mg^{2+} may be related to the weathering by hydrolysis of magnesium-rich minerals like $CaCO_3$, and $CaMg(CO_3)_2$, in addition to the anthropogenic sources such as the intensive agricultural activities in the study area (Alsuhaimi et al., 2019).

K^+ is commonly found in various rocks, thus, the high K^+ level in the GW is due to the relative solubility of K^+ bearing rocks. Thus, feldspar weathering of igneous rocks and weathering of silicate and clay minerals in sedimentary rocks cause the natural presence of K^+ in GW. Chemicals from industries as well as fertilizers are significant sources for the occurrence of K^+ in GW (Mallick et al., 2018). Generally, K^+ and Na^+ ions in the GW are associated with each other; however, the level of K^+ is lower than Na^+ (Alsuhaimi et al., 2019). The high K^+ level in the current study may be due to anthropogenic sources and seawater intrusion.

3.1.3. Trace elements analysis

Trace elements commonly form insoluble compounds that promote metals precipitation in an alkaline GW (El gawad et al., 2008). Twenty-two trace elements have been analyzed in this study. These were As, B, Li, Se, U, Al, Be, Cd, Cr, Ba, Cu, Pb, Mn, Mo, Ni, P, Sr, V, Zn, Fe, Co, and Ag. The mean values of these elements were less than WHO permissible drinking water guidelines. Table 2 presents a summary of the statistical analysis of the main trace elements in the soil samples. These values are below the regulatory limits of trace elements in soils recommended by (USDA, 2000).

3.2. Hydrogeochemical facies and general water quality diagrams

Hydrochemical properties of the GW are attributed to the GW resident time, lithology, geology, and water regional flow pattern (Alsuhaimi et al., 2019). Hydrochemical facies is utilized to analyze the chemical composition of GW and illustrate the origin and chemical water types (Othman, 2005). General water quality diagrams are a convenient method to describe the water types according to the ionic composition (Adimalla and Venkatayogi, 2018). According to the ratio of anion and cation in the GW, it is usually classified into three main groups, namely bicarbonate, sulfate, and chloride types (Alsuhaimi et al., 2019). AquaChem software is widely used to analyze, plot, and report aqueous geochemistry and water quality of the GW supply wells. The general distribution of the anions and cations in the GW is illustrated by a Piper diagram. Fig. 4A shows the water quality classifications within a Piper plot. Fig. 4B, C, and 4D show a Piper plot for all GW

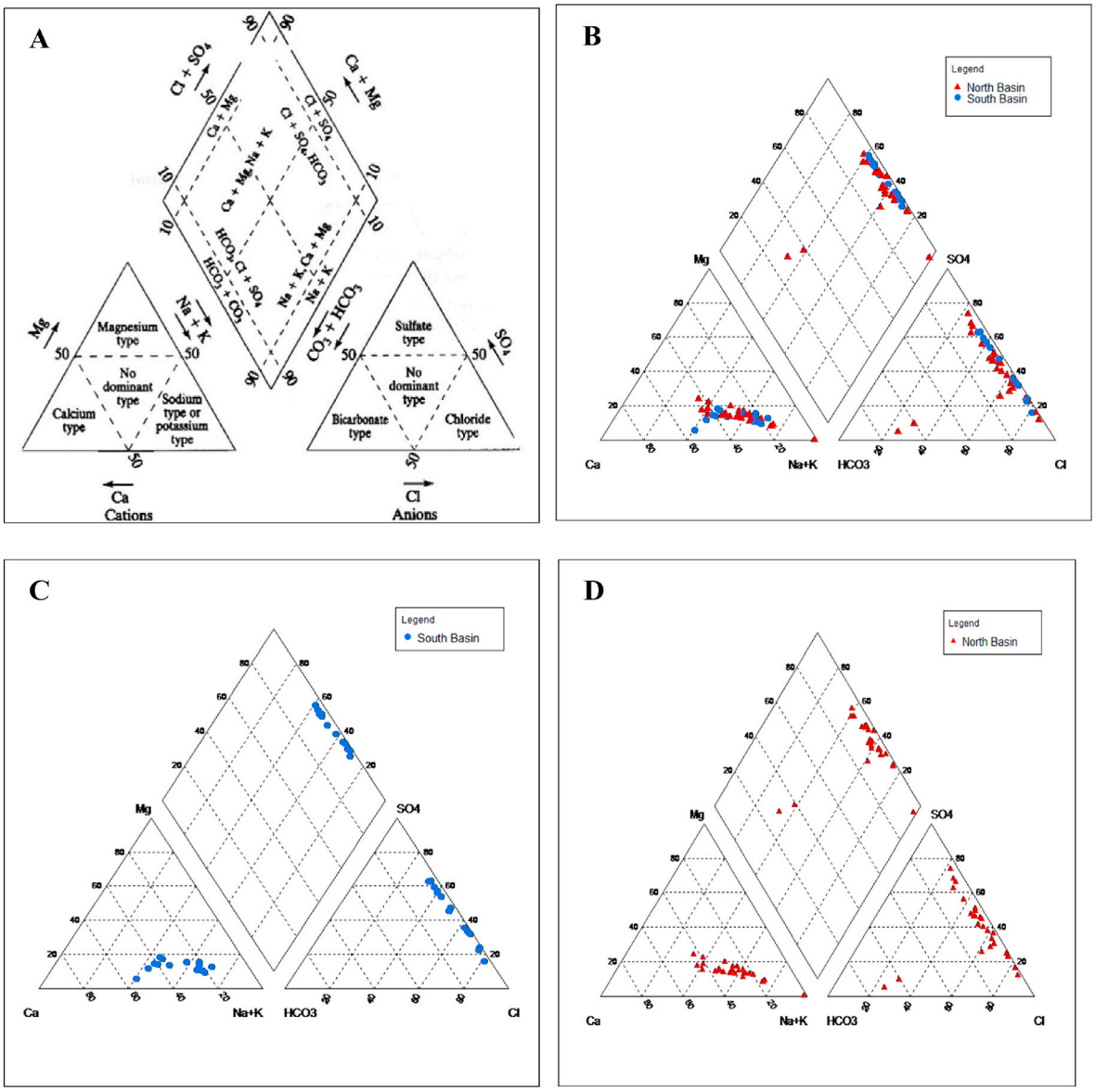

Fig. 4. Piper plots **A**. classification of water quality types, **B**. Piper plot for all GW samples, **C**. Piper plot for south basin samples, and **D**. Piper plot for north basin samples.

samples, south basin samples, and north basin samples, respectively. Fig. 5A, B, 5C, and 5D show the hydrogeochemical plots Schoeller, Durov, Ternary, and Ludwig Langelier plots respectively. These diagrams provide a "fingerprint" by plotting the common cations and anions. These diagrams allow an "at a glance" characterization of general water quality.

Piper plot shows that in the anion triangle, the GW samples range as chloride to sulfate type and only two samples are bicarbonate type. While in the cation triangle, the GW samples range as sodium and potassium type. As shown in the diamond-shaped part the analyzed GW samples are mostly found in SO_4–Cl and Ca–Mg (permanent hardness) part of calcium chloride type (non-carbonate hardness above 50%), and in the field of SO_4–Cl and Na–K (saline) of sodium chloride type (non-carbonate alkali above 50%) of water. Only two samples in the field of HCO_3–CO_3 and Ca–Mg (temporary hardness), magnesium bicarbonate $Mg(HCO_3)_2$ type (carbonate hardness above 50%), indicating the dissolution of rock-forming minerals like the dissolution of sulfate from gypsum and anhydrate and Na-rich carbonate rocks dissolution and halite. These results are consistent with the computed mean values of the mineral phase SI that shows under-saturation of halite, gypsum, and anhydrate and over-saturation of calcite and dolomite. These water types indicate the presence of ion exchange and reverse ion exchange reaction, deep brackish and seawater intrusion, and wastewater. The GW types are more variable in the north GW basin than in south basins. Two wells in the north GW basin showed magnesium-bicarbonate-type water, indicating high recharge by freshwater, whereas the most GW samples are dominated by the combination of sodium-chloride-type and calcium-sulfate-type. The calcium-bicarbonate-type waters were associated with the carbonate depositional facies of the Rus formation in the north of Qatar.

Similar trends were shown by the Ternary, Ludwig Langelier, Schoeller, and Durov diagrams. A high level of Cl^-, Na^+, and SO_4^{2-} and lower level of HCO_3^-, and Mg^{2+} ions in the GW samples was observed. The result is consistent with (Ghalib, 2017). Generally, Cl^- and SO_4^{2+} (strong acids) are dominant over CO_3^{2-} and HCO_3^- (weak acids), and Na^+ and K^+ were above Ca^{2+} and Mg^{2+} (alkaline earth elements) significantly. Thus, most GW samples were dominated by the combination of sodium-chloride-type and calcium-sulfate-type. The bicarbonate anion depleted relative to other anions except in some north GW basin samples with low salinity. Durov diagram results suggested the geochemical

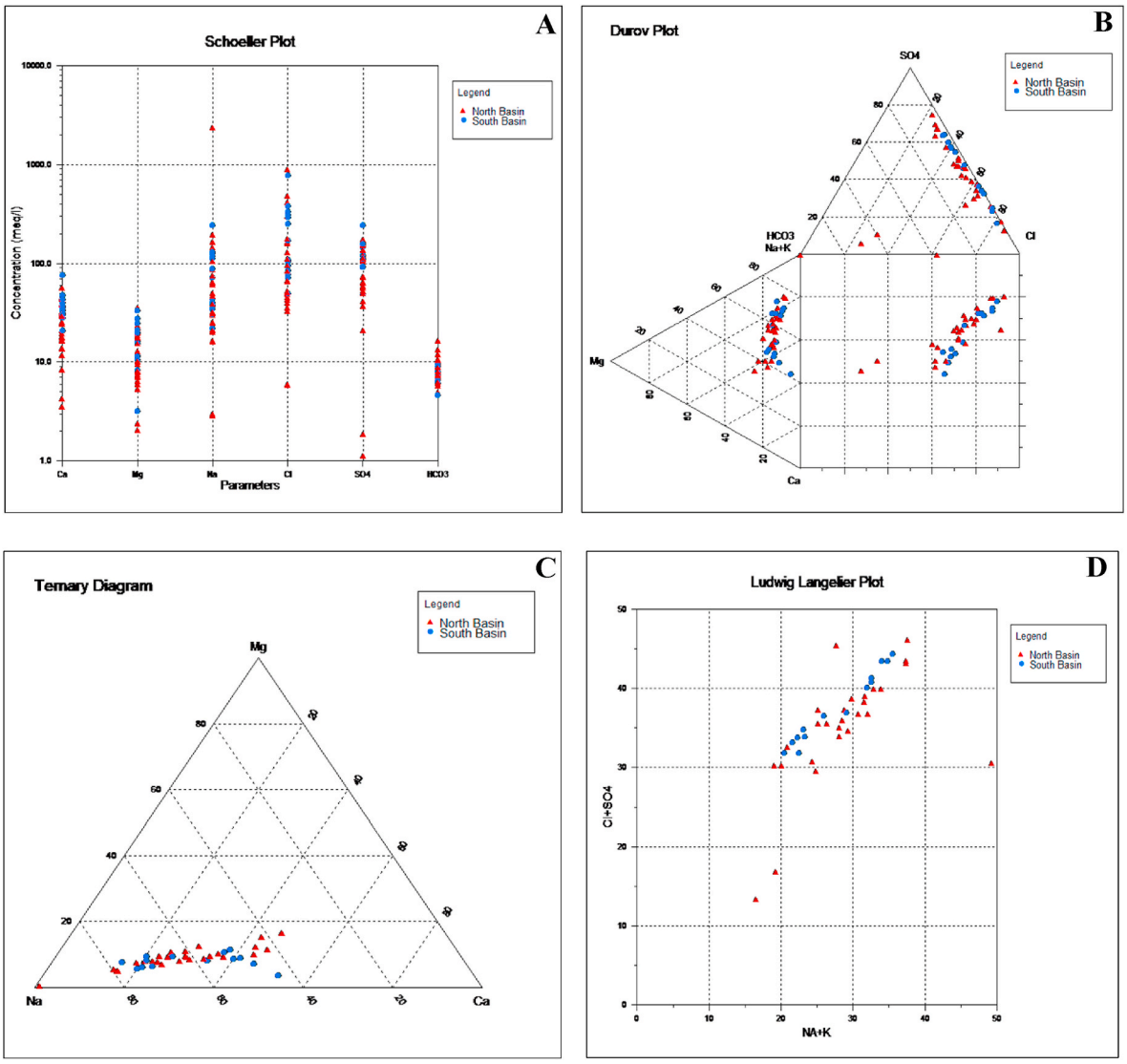

Fig. 5. Hydrogeochemical plots for the GW Samples **A**. Schoeller plot, **B**. Durov plot, **C**. Ternary plot, and **D**. Ludwig Langelier plot.

evolution where the rainfall recharges GW with Ca–HCO_3 water type then water flow goes through water-rock interactions and dissolution of minerals such as karst formation in Qatar with dolomite, limestone, and gypsum. This resulted in the formation of Ca–SO_4 and Na–SO_4 water types by ion exchange. Then the flow water mix with the pre-existing GW, which is mainly of high salinity in Qatar and finally reverse ion exchange lead to the formation of the Na–Cl and Ca–Cl type.

The stiff diagram (Appendix A) shows a vertical axis of sodium-chloride, calcium-bicarbonate, magnesium-sulfate, and iron-carbonate. The resulted polygonal-shaped illustrate the solute distribution in GW samples. Stiff diagrams results are consistent with piper plots showing four GW types. The stiff diagram shows that the main water type is sodium-chloride, which suggests the intrusion of the brackish water from the deep aquifer or adjacent seawater.

3.2.1. *Irrigation water quality and irrigation hazard diagrams*

The irrigation water problems, which are related to water quality, are salinity, trace elements, and a group of other miscellaneous problems such as nitrate. Othman (2005) stated that the sodium absorption ratio (SAR) could be used to calculate sodium hazard. SAR measures the extent to which sodium in water substitutes adsorbed calcium (Ca^{2+}) and magnesium (Mg^{2+}) or sodium molarity over calcium plus magnesium molarity as shown in equation (6).

$$\mathrm{SAR} = \frac{Na^{+}}{\sqrt{\frac{(Ca^{2+}+Mg^{2+}}{2}}} \tag{6}$$

where sodium, calcium, and magnesium levels are in milliequivalents/L.

Ranking of water suitability for irrigation can be done by using the irrigation hazard diagram (Wilcox plot) based on specific EC and SAR. The resulting four zones of alkalinity hazard are low sodium hazard water S1 (SAR < 10), medium sodium hazard water S2 (10 < SAR < 18), high sodium hazard water S3 (18 < SAR < 26), and very high sodium hazard water S4 (SAR > 26). While the resulting four zones of salinity hazard are low salinity Cl (EC < 250), medium salinity C2 (250 < EC < 750), high salinity C3 (750 < EC < 2250) and very high salinity C4 (EC > 2250).

Salinity problem causes the salts to accumulate in the crop root zone, decreases the osmotic of plants, hinders water from the plants, and causes a loss in yield (Machado and Serralheiro, 2017). Toxicity problems occur due to the high ion concentration that accumulates to significant levels and lead to crop damage or decreased yields. The level of damage depends on the absorbed amount and tolerability. Furthermore, toxicity commonly accompanies and complicates the salinity or water infiltration problem. Soil amendments might be needed for irrigation water with a high value of SAR to keep away the long-term soil

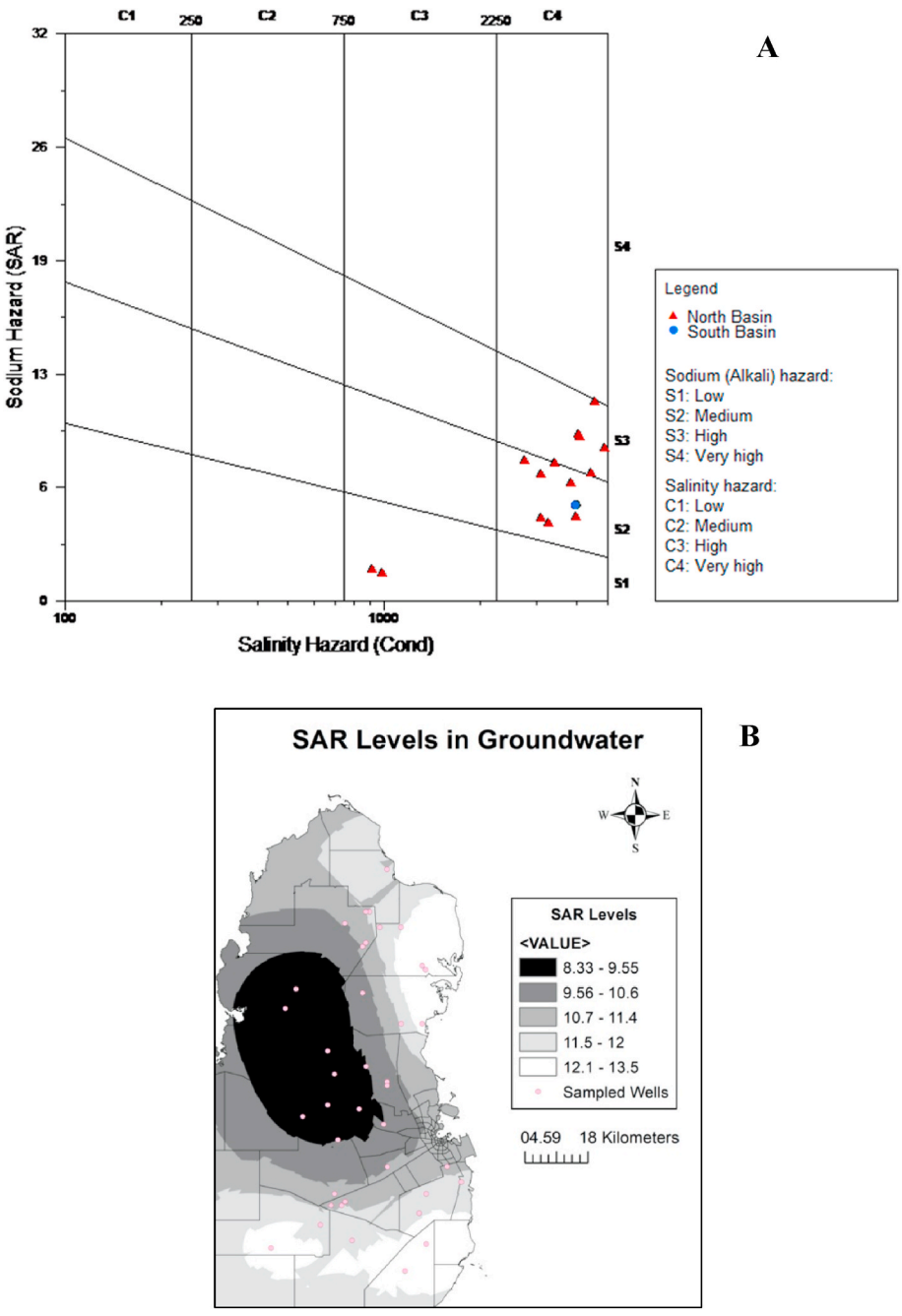

Fig. 6. A. Wilcox plot for groundwater samples, **B.** Interpolated map for SAR distribution in the study area.

degradation. Soil damage occurs due to Na^{+} ability in water to replace Ca^{2+} and Mg^{2+} in the soil. This will reduce the soil's ability to form stable aggregates and reduce the infiltration and permeability of the soil to water. However, sandy soils will have lower problems than clay soils (Sherif et al., 2011).

Samples in the irrigation hazard diagram (Wilcox plot) are grouped on the GW basins as shown in Fig. 6A. Notice that the irrigation hazard diagram is for specific electrical conductivity less than 5000 μS/cm. In the current study, only 16 samples (39%) have EC less than 5000 μS/cm. The irrigation hazard analysis indicates that irrigation use of 60.9% of the GW samples with specific electrical conductivity greater than 5000 μS/cm would not be expected since this would likely cause harm to agriculture. The high salinity is measured by specific electrical conductivity in the current study (mean values 5035 μS/cm) indicating that the GW with high salinity is not suitable for irrigation and it is only suitable for salt tolerance and semi tolerant crops. Wilcox plot shows 16 samples (34%) fall into the category of C4S2 and C4S3, indicating a very high salinity hazard and medium sodium hazard, and very high salinity hazard and high sodium hazard, respectively. The result shows that the irrigation hazard is always higher from salinity than from SAR. According to Ghalib (2017), C4 category GW samples are not suitable for irrigation for all soil types except for high permeable soil. Only two samples (4.8%) fell into high salinity and low alkalinity hazard (C3S1 category), which would not be expected to likely cause infiltration problems that the higher the salinity, the higher the SAR index so that the infiltration problems could happen. Using the S1 category for irrigation purposes is suitable for types of soil having slight risk or no risk of Na^{+} replacement, such as using coarse soil or organic soils with significant permeability (Adimalla and Venkatayogi, 2018). The C3 category might be used for irrigation semi-tolerant crops (Marghade et al., 2011).

Table 3
Summary of the statistical analysis using the PHREEQC and the calculated saturation indices (SI) of the collected GW samples with respect to some common minerals.

Mineral	Minimum (SI)	Maximum (SI)	Mean (SI)	Median (SI)
Anhydrite	−2.108	0.311	−0.290	−0.132
Barite	−0.453	0.349	0.047	0.058
Calcite	−0.787	0.618	−0.186	−0.189
Dolomite	−1.179	1.126	−0.592	−0.697
Fluorite	−0.526	1.114	0.213	0.215
Gypsum	−1.871	0.530	−0.059	0.102

The SAR distribution for the study area is illustrated in Fig. 6B. The distribution map shows high SAR values in the coastal areas.

The SAR plot only shows the impact of sodium on the stability of soil aggregates. However, high K^+ and Mg^{2+} ion levels have also negative impacts on the soil permeability. For example, Mg^{2+} in water impacts the soil by enhancing the alkalinity and reducing the crop yield. Another problem related to irrigation water quality occurs with high nitrate concentrations, which may cause extreme vegetable growth, lodging, and retarded crop maturity. High nitrate may indicate anthropogenic impact from inorganic and organic fertilizers, slurry from animal production, and domestic effluents. Alfy et al. (2017) stated that boron occurs naturally in GW due to boron desorption by infiltrating rainwater from mineral surfaces. This might increase the boron levels by an ion exchange, which is accompanied by Ca depletion and Na enrichment. The high boron concentrations are often caused by infiltrating wastewater, which has high boron from soaps and detergents.

3.2.2. Hydrogeochemical saturation index (PHREEQC analysis)

PHREEQC analysis was done to calculate saturation indices for various minerals, evaporite (gypsum, anhydrite, and halite), carbonate (calcite and dolomite), fluorite, and barite found in the aquifer to determine whether there is a tendency towards precipitation or dissolution. The summary of the statistical analysis using the PHREEQC and the calculated saturation indices (SI) of the collected GW samples with respect to some common minerals are shown in Table 3. The geochemical modeling program PHREEQC, integrated in AquaChem, is used to compute the saturation indices of common minerals. For the current study, the most relevant output of the geochemical modeling program PHREEQC is the mineral saturation indices, which express the tendency of a solution to dissolve or to precipitate minerals based on its chemical composition, pH, redox potential and temperature. The saturation index was calculated for each mineral. If the saturation index values are in the range of −0.5 to +0.5; then this should pose no potential risk of dissolution or precipitation. If a negative value of the SI, which is less than −0.5, then this suggests that the solution is undersaturated with respect to the mineral and shows a tendency of the solution to dissolve the mineral if it is present in the aquifer. A positive SI, which is greater than +0.5, then this indicates over-saturation and the solution tends to precipitate the mineral. The SI of approximately 0 indicates equilibrium or saturation conditions between the solution and the mineral and no reaction is expected to occur.

Fig. 7A, B, and 7C illustrate the calculated SI for all GW samples, north basin samples, and south basin samples respectively. Undersaturation with respect to evaporites such as halite (NaCl), anhydrate ($CaSO_4$), and gypsum ($CaSO_4{\cdot}2H_2O$) were found. While over-saturation

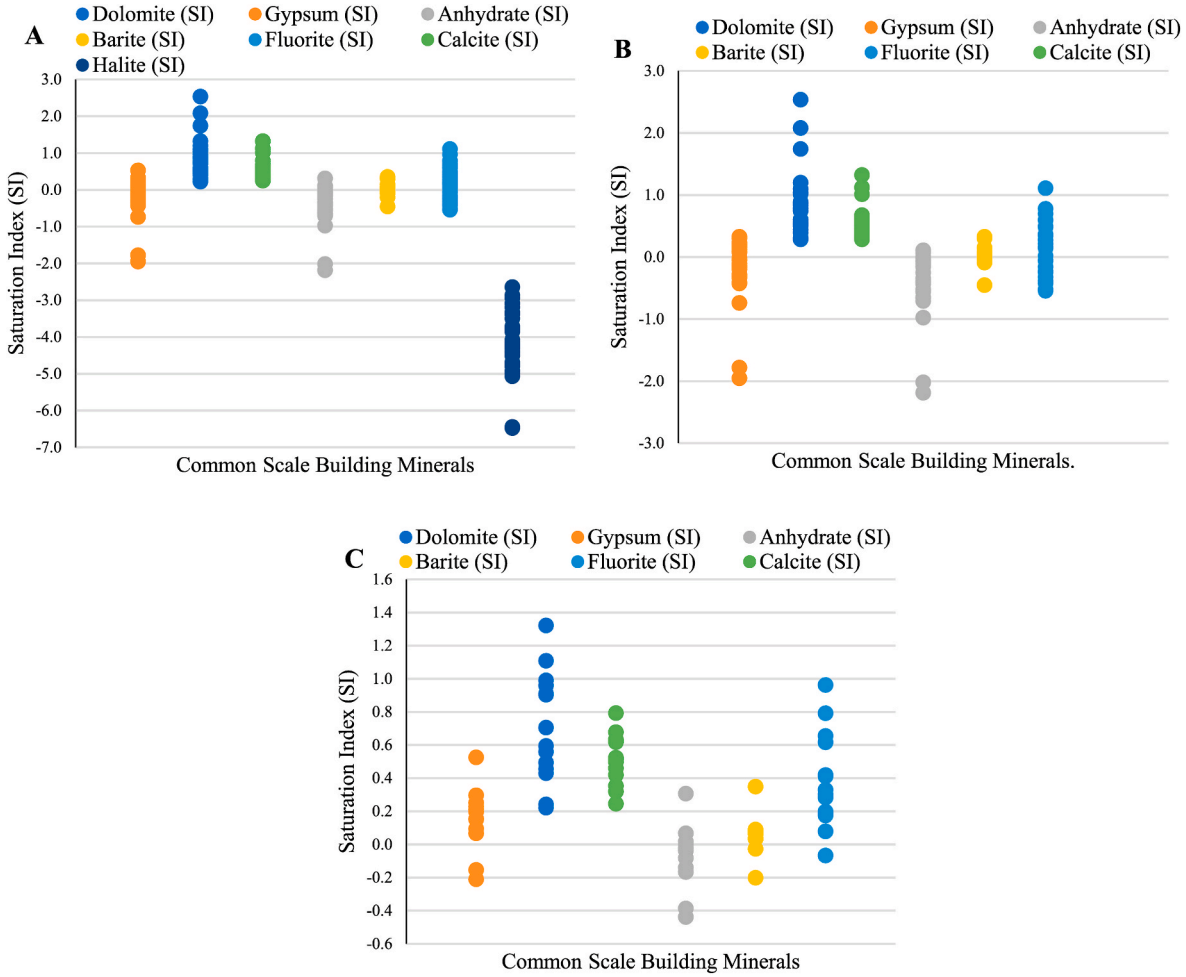

Fig. 7. A. Saturation indices (SI) of all sample locations, **B.** SI for the north basin, and **C.** SI for the south basin.

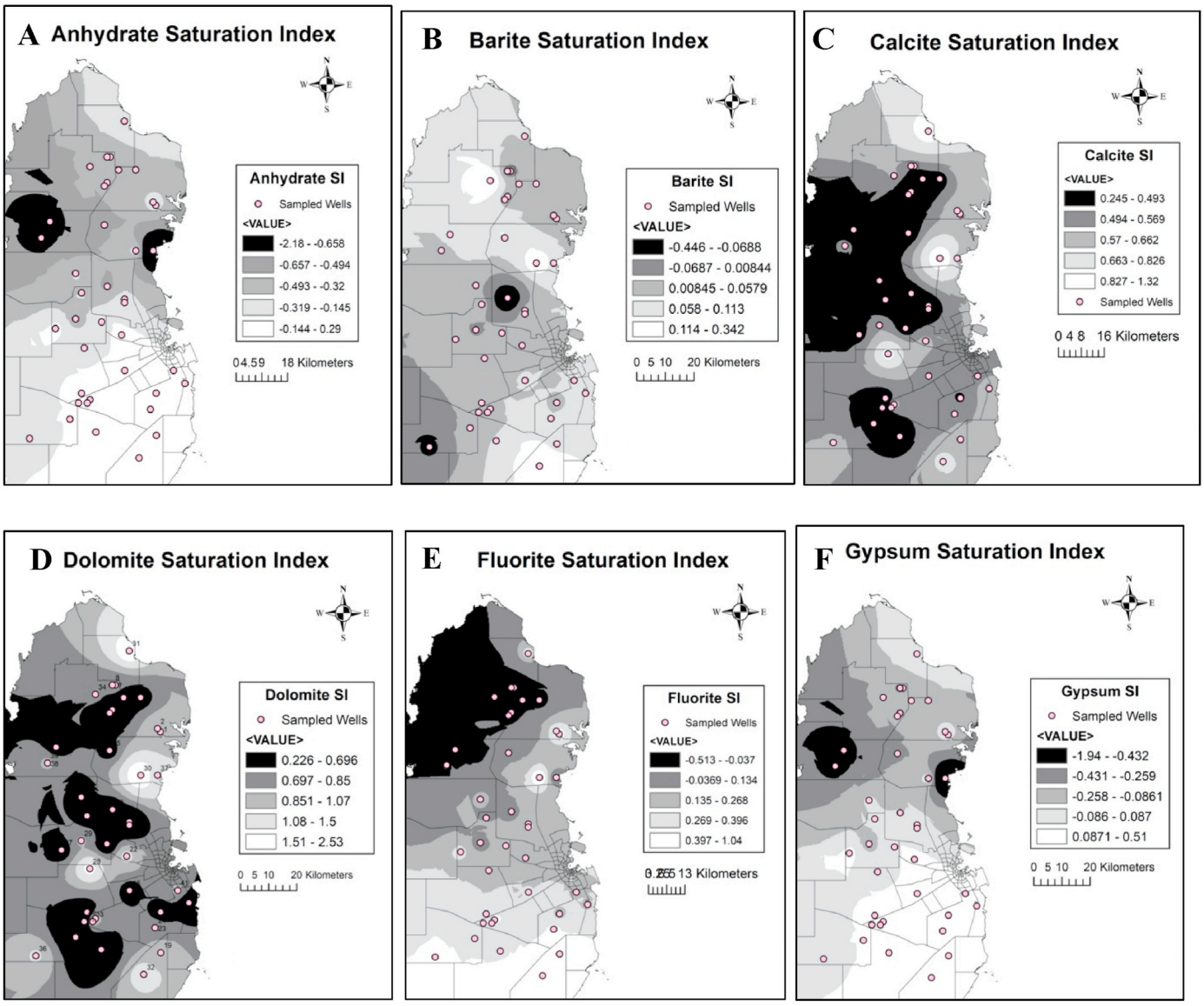

Fig. 8. Interpolation maps of **A**. anhydrate, **B**. barite, **C**. calcite, **D**. dolomite, **E**. fluorite, and **F**. gypsum.

of carbonate like dolomite $CaMg(CO_3)_2$, fluorite (CaF_2), and calcite ($CaCO_3$) is shown in Fig. 8. The areas with the most positive SI values would have the greatest potential for precipitation of these minerals; however, precipitation of dolomite (dolomization) is not observed to occur and dolomite is known to precipitate very slowly (SWS, 2009). These results indicate that the carbonate precipitation is significantly attributed to the evaporite dissolution. Adimalla and Venkatayogi (2018) stated that significant levels of SO_4^{2-} and Ca^{2+} that might precipitate to the soil, and $CaCO_3$ saturation was observed in the semi-arid and arid area of sub-surface and surface water.

The areas with the most negative halite, anhydrate, and gypsum SI values would have the greatest potential for dissolution of these minerals, which tend to be in the dissolved phases indicating an increase Cl^-, SO_4^{2-} and salinity in GW with water flow. Calcite at first rapidly dissolute by rainwater in comparison with dolomite, then the GW is oversaturated by calcite as Ca^{2+}, CO_3^{2-} and HCO_3^- levels increase. Permeability and porosity of an aquifer can be enhanced by the dissolution of these minerals causing fractures enlargement in the aquifer. This suggestion is consistent with the presence of karst formation in Qatar. The result of the saturation indices and the minerals trends are consistent with the sodium, chloride, calcium, and sulfate levels in GW as shown by the interpolation maps in Fig. 8. The areas with higher calcium indices have a greater likelihood of well-scaling problems. Interpolated maps for anhydrate, barite, calcite, dolomite, fluorite, and gypsum are presented in Fig. 8.

3.3. Statistical analysis

Descriptive statistics and correlation analysis were computed using the statistical package for the social sciences (SPSS). The physiochemical variables were analyzed for the 41 water samples. Table 1 shows the summary of the statistical analysis (maximum, minimum, mean as well as the standard deviation values) of the physicochemical characteristics of the GW samples. Outliers could be used as an indicator of potential agricultural activities such as fertilizer impacts, localized hydrostratigraphic, geochemical conditions, or impacts from the well itself. For example, the highest specific electrical conductivity readings were in coastal areas, and the lowest readings were in central of Qatar. Another example, fluoride, sulfate, strontium, selenium, and boron could be correlated with evaporite deposits, whereas nitrate could be correlated with fertilizer impacts. If nitrogen levels in drinking water exceed the permissible limits, it can cause infant methemoglobinemia (blue-baby

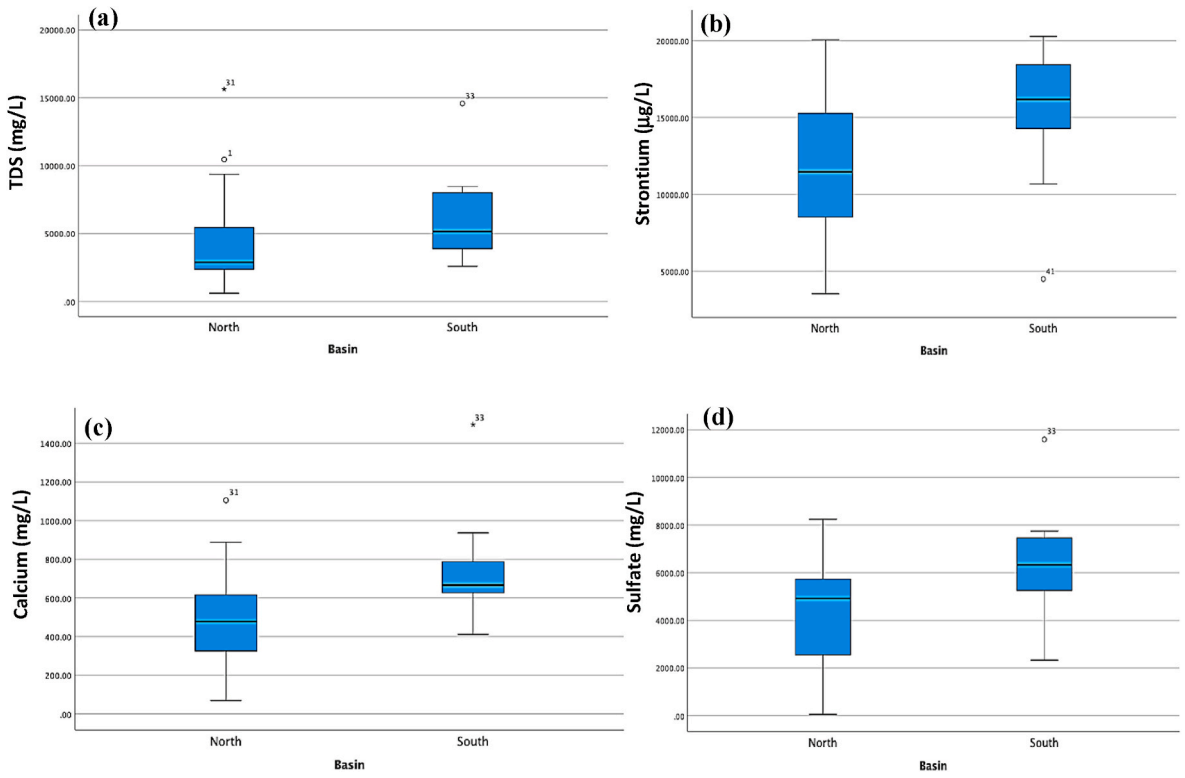

Fig. 9. Mean difference between groundwater basins of (**a**) TDS (mg/L), (**b**) Strontium (µg/L), (**c**) Calcium (mg/L), and (**d**) Sulfate (mg/L).

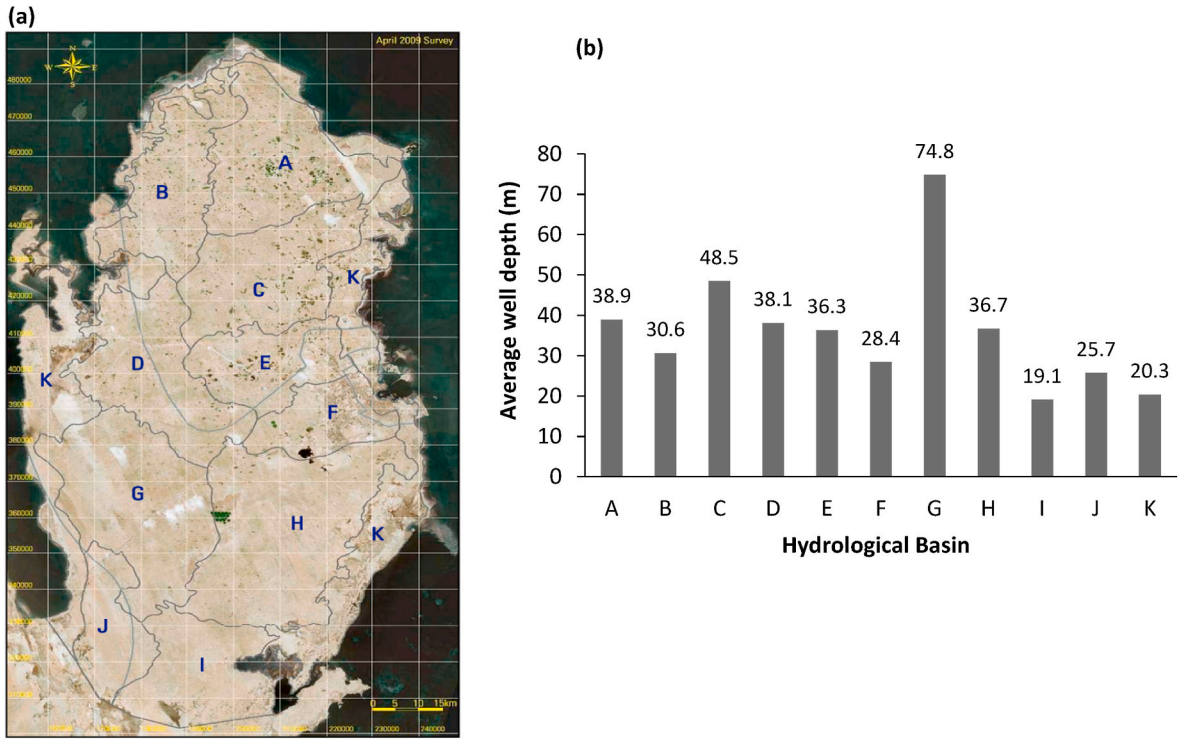

Fig. 10. **(a)** Hydrological basin for the state of Qatar and **(b)** Average well depth by the hydrological basins.

syndrome), birth malformations, goiter, gastric cancer, hypertension, metabolic disorder, and livestock poisoning. Furthermore, arsenic, iron, manganese, and molybdenum could be associated with a localized sedimentary depositional or hydrogeochemical environment.

To test the statistical differences between sample means in different locations, the wells were categorized according to the GW basins (north and south GW basin) and according to the hydrological basins. To compare means between north and south GW basin, t-tests were applied, while one-way ANOVA (complete randomized design) was used to test the hypothesis of equal mean between hydrological basins. The results

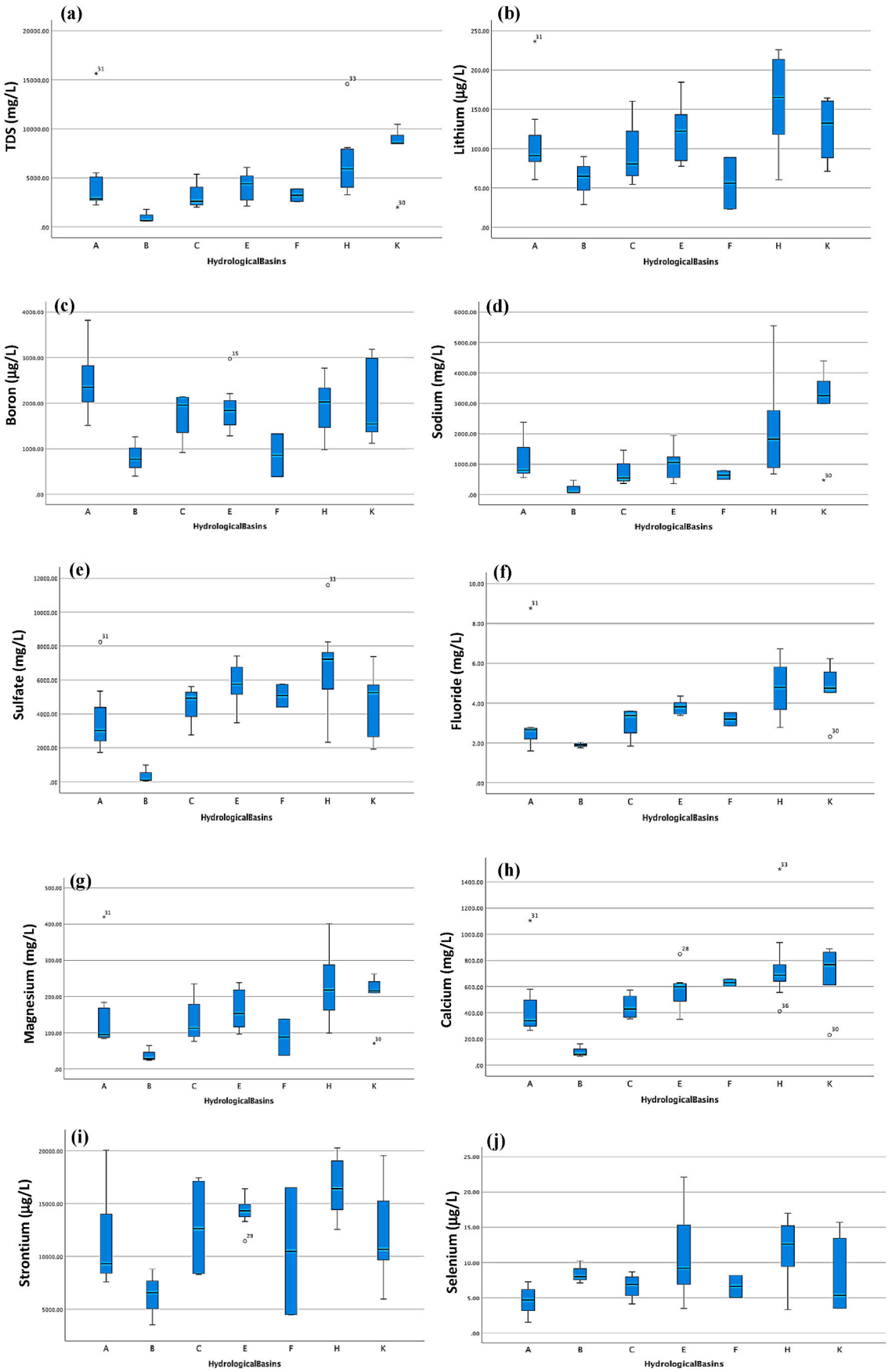

Fig. 11. Means difference between hydrological basins for **(a)** TDS (mg/L), **(b)** Lithium (µg/L), **(c)** Boron (ppb), **(d)** Sodium (mg/L), **(e)** Sulfate (mg/L), **(f)** Fluoride (mg/L), **(g)** Magnesium (mg/L), **(h)** Calcium (mg/L), **(i)** Strontium (µg/L), and **(j)** Selenium (µg/L).

show that TDS does not differ from the north basin to the south basin as shown in Fig. 9a. The results show that for strontium, calcium, and sulfate, the p-value is < 0.05. The data provided sufficient evidence to support that there is a difference in strontium, calcium, and sulfate means between the north basin and south basin as shown in Fig. 9b, c, and 9d, respectively.

According to SWS (2009), the hydrological basins categories were based on the surface water runoff in Qatar. These include 11 areas from A to K as shown in Fig. 10a. Area K consists of the entire perimeter of the Qatar peninsula and includes most of the coastal. The well total depth was measured and the average well depths by hydrological basins are shown in Fig. 10b.

The ANOVA results for the TDS, lithium, boron, sodium, sulfate, fluoride, magnesium, calcium, strontium, and selenium are shown in Fig. 11. The statistical ANOVA results for the TDS, lithium, boron, sodium, sulfate, fluoride, magnesium, calcium, strontium, and selenium showed that the p-value was less than 0.05 as shown in appendix B (t-tests & ANOVA Test). From the TDS homogenous subsets, the mean of hydrological basin B is not under the same column with the mean of hydrological basin K, which means they are not homogenous. Therefore, the mean of hydrological basin K is significantly different from the mean of hydrological basin B at a 95% confidence interval.

It was noticed that the lithium interval values of the hydrological basin H versus the hydrological basin B (0.43, 199) did not contain zero and that p-value was less than 0.05. Therefore, the mean of hydrological basin H is significantly different from the mean of hydrological basin B at a 95% confidence interval. Boron mean of hydrological basin A is significantly different from the mean of hydrological basin B and F at 95% confidence interval. The sodium mean of the hydrological basin k was significantly different from the mean of the hydrological basins A, B, C, E, and F at 95% confidence interval. The sulfate mean of the hydrological basins A and B versus the hydrological basins C, K, F, E, and H and the hydrological basin at a 95% confidence interval. The fluoride mean of the hydrological basin B is significantly different from the mean of hydrological basin H at a 95% confidence interval. Magnesium mean of the hydrological basin B is significantly different from the mean of the hydrological basin H at a 95% confidence interval. The calcium mean of the hydrological basin B was significantly different from the mean of the hydrological basins E, F, K, and H, at a 95% confidence interval. The strontium mean of hydrological basin H was significantly different from the mean of hydrological basin A and B, and the hydrological basin B versus the hydrological basins E, at a 95% confidence interval. The selenium mean of the hydrological basin A is significantly different from the mean of the hydrological basins E and H at a 95% confidence interval. The ANOVA results showed that TDS, lithium, boron, sodium, sulfate, fluoride, magnesium, calcium, strontium and selenium are correlated with the GW depth.

Regression analysis and Pearson correlation were used to check the correlation between water physiochemical parameters such as temperature, pH, TDS, TOC, total hardness (TH), major cations and anions, and trace metals for different GW and topsoil samples. The term strongly correlation refers to $r > 0.7$, moderately correlation refers to $r = 0.5$–0.7 and weakly correlations refer to $r < 0.5$. The results of significant regression correlations are shown in appendix B (t-tests & ANOVA).

The correlation and regression analysis showed that concentrations of the major anions and cations namely sodium, chloride, calcium, potassium, magnesium, fluoride, bromide, and sulfate were a strong predictor for TDS in the GW. Also, the GW salinity was strongly correlated with the GW constituents which exceeded water quality guidelines, namely lithium, boron, molybdenum, strontium, uranium, chromium, selenium and anions and cations namely sodium, chloride, calcium, potassium, magnesium, fluoride, bromide and sulfate with highly significant p-value and strong correlation with a correlation coefficient of 0.999. These correlations show that these are the main constituents that increase the GW salinity. The results of sulfate salts and evaporite minerals dissolution are consistent with (Mallick et al., 2018) such that

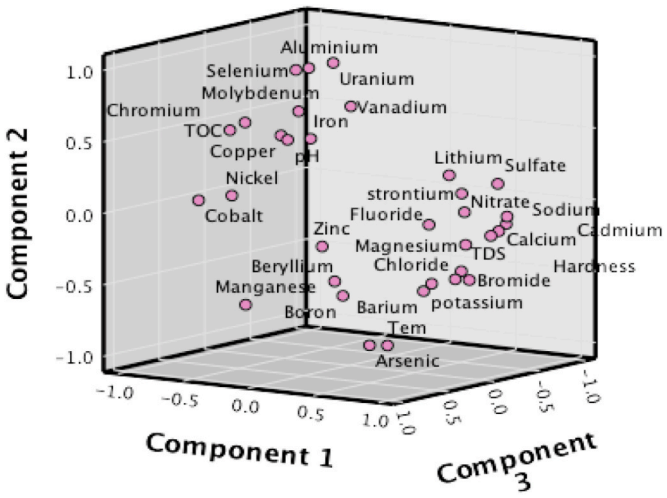

Fig. 12. Principle component analysis plot.

they are more favorable by the highly saline GW, which causes the levels of Mg^{2+} and Ca^{2+} to increase.

Anions and cations namely sodium, chloride, calcium, potassium, magnesium, fluoride, bromide, and sulfate are strongly correlated to each other which contributes to the GW salinity and mineralization. The results were consistent with the SI calculated showing that the dissolution/precipitation caused the concurrent increase/decrease in the cations/anions (Al-Kalbani and Price, 2015). For example, the correlation between Cl^- and Na^+ was consistent with the dissolution of the halite; SO_4^{2-} correlated with Na^+, Ca^{2+}, and Mg^{2+}; indicating the dissolution of evaporite minerals. The correlation between Ca^{2+} and SO_4^{2-} contributed to gypsum dissolution, also the correlation between Ca^{2+} and Mg^{2+} infers the dolomite dissolution with low content of magnesium carbonate. A good correlation between Ca^{2+}, Mg^{2+}, Na^+, and K^+ levels in the GW suggests a common source for the major cations. High fluoride levels in GW are commonly dissolution by hydrolysis or removed by precipitation of calcite, which is consistent with (Alfy et al., 2017).

The correlation between the Cl^- and SO_4^{2-} with Na^+, K^+, Ca^{2+}, and Mg^{2+} is consistent with the hydrochemical facies analysis as most of the GW samples were dominated by the combination of sodium-chloride-type and calcium-sulfate-type. The correlation between total hardness and the ions Ca^{2+}, Mg^{2+}, and Cl^- showed that the hardness of the water was permanent in nature. The effect of the ion exchange process is indicated by the relations between Na^+ and K^+ with Mg^{2+} and Ca^{2+}.

The multiple regression analysis showed a highly significant correlation between lithium and boron and molybdenum, and a good correlation with a correlation coefficient of 0.601. Boron and lithium in water did not show a significant correlation with boron and lithium in topsoil concentrations. The significant correlation was between sodium and chromium concentration in water with sodium and chromium concentrations in topsoil.

PCA is a significant method to recognize patterns and analyze the variance of a big set of inter-correlated variables and to extract the Eigenvalues and Eigenvectors (loadings) for PCs from their associated variance (Ravikumar and Somashekar, 2015). PCA represents the dimensional of the large dataset, increase interpretability, and decrease the loss information (Jolliffe and Cadima, 2016). Fig. 12 shows the PCA plot. The results of the principal component analysis are shown in appendix C.

It suggests three significant PCs, of Eigenvalues higher than one, explain 99% of the total variance of the dataset. All loadings, greater than 0.6, are considered in interpreting the analysis as a significant contributor. The first principal component (PC1) explains 49% of the total variance. PC1 showed a positive loading of Mg, TH, Sr, Ca, TDS, SO_4, Li, Cl, F, Br, Cd, K, Ba, Na, representing the factors, which are

Table 4
Comparison results of the general water quality parameters with the national and international standards and guidelines.

Parameter	Number & frequency of detection	Min	Max	Mean	Number of exceedances	WHO (WHO, 2017)		USEPA		QATAR & GSO (GSO, 2008)	
						Drinking-Water	Irrigation Water	Drinking-Water	Irrigation Water	Drinking-Water	Irrigation Water (FAO, 1994)
General Water Quality Parameters											
pH	41 100%	6.89	7.94	7.3	–	6.5–8.5	–	6.5–8.5	6.5–8.5	6.5–8.5	6–8.5
Electrical Conductivity (EC), µS/cm	41 100%	920	22330	7298.8	39 > 1200 38 > 3000	1200	–	–	–	–	3000
Total Dissolved Solids (TDS), mg/L	41 100%	598.87	15633	5109.2	41 > 500 39 > 1000 38 > 2000	1000	–	500	2000	1000	2000
Hardness, mg $CaCO_3$/L	41 100%	275.2	5393	2120	41 > 120 39 > 500	500 ***	–	–	–	–	120
Total Organic Carbon (TOC), mg/L	41 100%	1.27	35.50	14.62	–	–	–	–	–	–	75
Anions and Cations											
Calcium (Ca^{2+}), mg/L	41 100%	69.94	14978	570.2	40 > 80 35 > 300 29 > 400	300 ***	–	–	–	80 **	400
Magnesium (Mg^{2+}), mg/L	41 100%	24.41	420.2	169.1	39 > 30 38 > 60	–	–	–	–	30 **	60
Sodium (Na^{+}), mg/L	41 100%	64.22	5547.1	1466.48	41 > 60 39 > 80 39 > 200 20 > 920	200 ***	–	60	–	80 **	920
Potassium (K^{+}), mg/L	41 100%	16.36	320	90.18	41 > 2 41 > 4	–	–	–	–	4 **	2
Fluoride (F^{-}), mg/L	41 100%	1.59	8.77	3.81	41 > 1 41 > 1.5 14 > 4	1.5	–	4	1	1.5	15
Chloride (Cl^{-}), mg/L	41 100%	203.68	30807	6289.5	41 > 80 35 > 300 39 > 1059	250		250	–	80 **	1059
Bromide (Br^{-}), mg/L	41 100%	0.37	21.98	4.32	41 > 0.1	–	–	–	–	0.1**	–
Nitrate (NO_3^{-}), mg/L	41 100%	0.00	113.34	36.32	36 > 10 10 > 50	50	–	10	–	50	10
Sulfate (SO_4^{2-}), mg/L	41 100%	53.46	11596	4977.2	41 > 50 39 > 250 39 > 400	250 ***	–	250	–	50 **	400
Boron, mg/L	41 100%	0.388	3.819	1.884	39 > 0.75 20 > 2 8 > 2.4 3 > 3	2.4	–	6 *	2 Long term use 0.75 short term use	2.4	3
Lithium, mg/L	41 100%	0.023	0.236	0.1205	39 > 0.05	–	–	–	2.5	0.05	–
Molybdenum, mg/L	41 100%	0.0078	0.293	0.0538	9 > 0.07 23 > 0.04 18 > 0.05 40 > 0.01	0.07	–	0.04*	0.05 Long term use 0.01 short term use	0.07	–
Selenium, mg/L	41 100%	0.00154	0.022	0.0088	1 > 0.02	0.04	–	0.05	0.02	0.04	–
Uranium, mg/L	41 100%	0.00011	0.031	0.0016	1 > 0.02 1 > 0.03	0.03	–	0.02	–	0.03	–
Chromium, mg/L	41 100%	0.0001	0.0118	0.0039	2 > 0.01	0.05	–	0.1	1 Long term use 0.1 short term use	0.05	For crop 0.01 For grass 0.2
Strontium, mg/L	41 100%	3.53	20.27	13.22	40 > 4	–	–	4 *	–	4	–
Aluminum, mg/L	10 24%	0.00015	0.0076	0.0015	–	0.2	5	0.2 mg/l	20 Long term use 5 short term use	0.2 **	15
Copper, mg/L	41 100%	0.00008	0.0044	0.00137	–	2	–	1.3	5 Long term use 0.2 short term use	2	For crop 0.2 for grass 0.5

(*continued on next page*)

Table 4 (*continued*)

Parameter	Number & frequency of detection	Min	Max	Mean	Number of exceedances	WHO (WHO, 2017)		USEPA		QATAR & GSO (GSO, 2008)	
						Drinking-Water	Irrigation Water	Drinking-Water	Irrigation Water	Drinking-Water	Irrigation Water (FAO, 1994)
General Water Quality Parameters											
Cobalt, mg/L	41 100%	<dl	0.0005	0.00007	–	–	–	–	5 Long term use 0.05 short term use	0.002	0.2
Iron, mg/L	38 29%	0.00001	0.118	0.0047	–	–	–	0.3	20 Long term use 5 short term use	0.3 **	1
Manganese, mg/L	41 100%	<dl	0.0049	0.001	–	0.4	–	0.03 *	10 Long term use 0.2 short term use	0.4	0.05
Cadmium, mg/L	31 75%	<dl	0.0005	0.000072	–	0.003	–	0.005	0.05 Long term use 0.01 short term use	0.003	0.05
Lead, mg/L	0	<dl	<dl		–	0.01	–	0.015	10 Long term use 5 short term use	0.01	0.1
Barium, mg/L	41 100%	0.003	0.0246	0.01	–	1.3	–	2	–	0.7	2
Beryllium, mg/L	13 31%	<dl	0.00014	0.00008	–	–	–	0.004	0.5 Long term use 0.1 short term use	0.004 **	–
Silver, mg/L		<dl	<dl		–	–	–	0.1	–	0.1 **	–
Arsenic, mg/L	41 100%	0.0006	0.005	0.002	–	0.01	.05	0.01	2 Long term use 0.1 short term use	0.01	0.1
Nickel, mg/L	41 100%	0.00024	0.0116	0.0019	–	0.02	–	0.1*	2 Long term use 0.2 short term use	0.07	For crop 0.2 for grass 0.5
Zinc, mg/L	20 48%	0.00003	0.0512	0.00588	–	3	–	5	2	3 **	0.5

Note * Lifetime risk health advisory, ** KAHRAMAA requirements for water quality distribution system, *** Taste threshold, dl: detection limit.

contributed to the high salinity of the GW due to the salt water intrusion and the mineralization of rocks and soil. For example, the positive loadings of Cl^- and SO_4^{2-} indicate the dissolution of evaporite minerals (halite (NaCl) and gypsum ($CaSO_4{\cdot}2H_2O$) which is supported by water type classification and SI calculations.

Moreover, 31% of the total variance is explained by the second principal component (PC2). PC2 showed the negative loadings of U, Al, Se, Se, Mo, Mg, and temperature, which could be associated with localized sedimentary depositional or hydrogeochemical environment. The third principal component (PC3) accounts for 19.9% of the total variance. PC3 shows positive loadings of Ni, Zn, Be, pH, Cu, Co, Fe, B, V, TOC that indicate the dissolution and precipitation (reducing and oxidizing factor). Only NO_3^- in PC3 was shown a high negative loading, which might indicate human influence from intense agricultural activities such as the utilization of potassium nitrate and phosphate fertilizers on quality of GW; particularly, potassium nitrate, which has high water solubility (Alfy et al., 2017). Therefore, there might be a vulnerability to anthropogenic pollution in a shallow aquifer. Knowing that boron and lithium are used as geothermal tracers (Al-Farraj et al., 2013). The positive loadings of boron and lithium might indicate a geothermal activity and mineral weathering. This is consistent with the high-significant positive regression correlation between sodium with boron and lithium.

3.4. Comparisons with standard and guidelines

The summary of the analytical results of the general water quality parameters, major cations and anions, and inorganic chemical concentrations are compared with the US environmental protection agency (US-EPA), the world health organization (WHO) and the Gulf standardization organization (GSO) drinking water and irrigation guidelines and standards as shown in Table 4. The mean values of the EC, TDS, hardness, cations, and anions namely Ca^{2+}, Mg^{2+}, K^+, Na^+, Cl^-, F^- and SO_4^{2-} exceeded the drinking and irrigation guidelines. All other means of water quality variables are within the guidelines. The interpolation maps for boron, lithium, molybdenum, strontium, chromium, and selenium are presented in Fig. 13.

Boron levels in eight samples exceeded the WHO, GSO, and Qatar drinking water guidelines. The presence of boron in GW can be naturally or due to anthropogenic sources. Natural sources are igneous rocks weathering and leaching from sedimentary boron-bearing salt deposits. Another natural boron source in the coastal regions due to its high volatility is rainfall containing sea salt from ocean spray. Anthropogenic sources are landfill leachate, drainage from coal mines and mining industry, glass industry, semiconductor manufacture, fly ash, petroleum products, using fertilizers or pesticides in agricultural, and sewage effluents due to using of sodium perborate in detergents and cosmetics

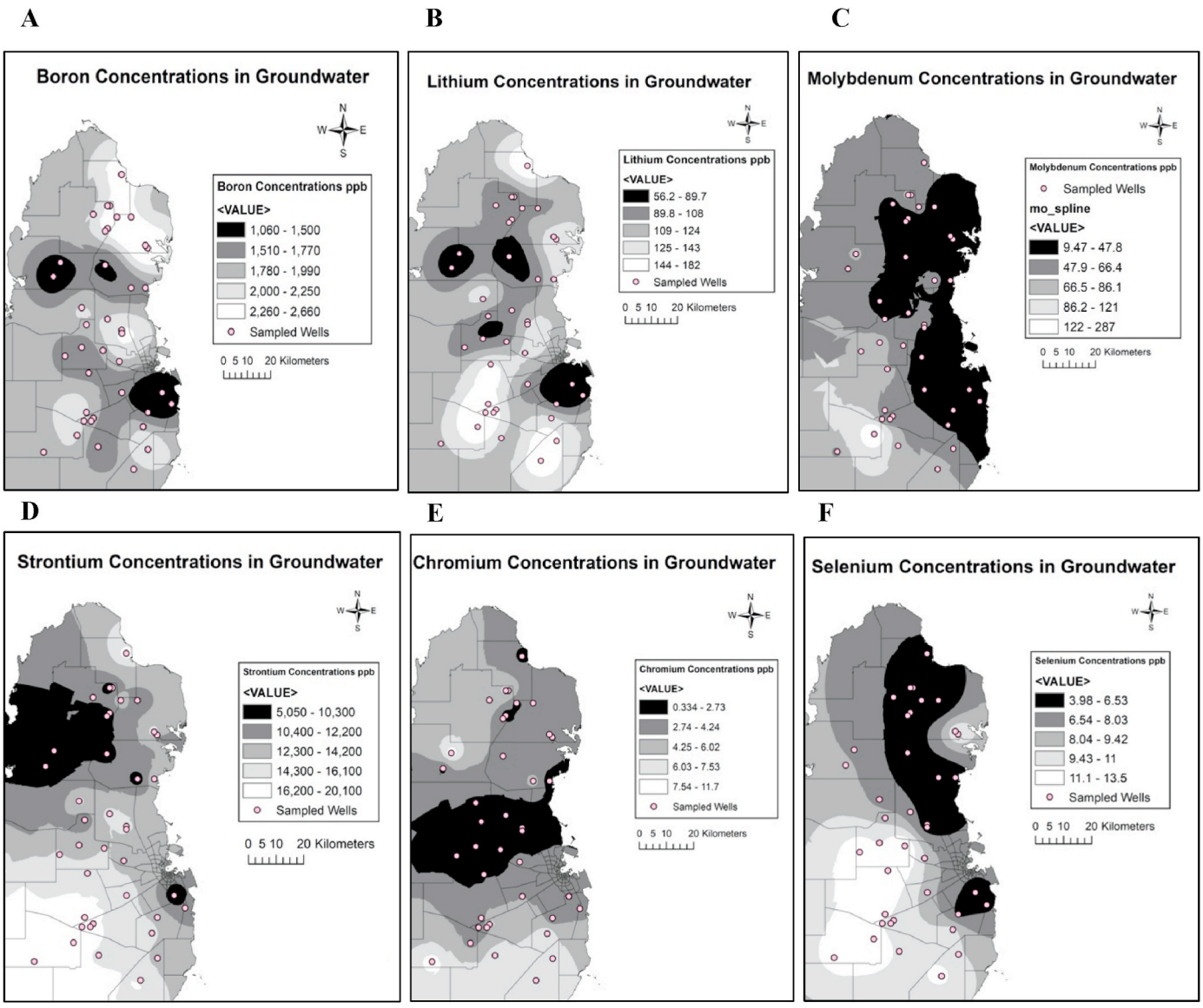

Fig. 13. Interpolation maps for **A**. Boron, **B**. Lithium, **C**. Molybdenum, **D**. Strontium, **E**. Chromium, and **F**. Selenium.

(Hasenmueller and Criss, 2013). In the current study, the anthropogenic sources of boron could be from the petroleum industry, using fertilizers or pesticides in agricultural, and sewage effluents. When boron amount is higher than required, toxic effects appear such as yellow tips of leaves, spots on fruits, spoil, and drop of unripe fruit, further it may cause the death of plants. Boron level less than 1 mg/L should be used in irrigation water for sensitive crops, and of a level of 0.5 mg/L for long-term irrigation (Voutsa et al., 2009). Boron forms complexes with other toxic metals such as lead, cadmium, or nickel, which may enhance the toxicity (Al-Ghouti et al., 2017).

Molybdenum levels in nine samples exceeded the WHO, GSO, and Qatar drinking water guidelines, and 23 samples exceeded the US-EPA lifetime health advisory. Mainly molybdenum compounds are low soluble in water, while when molybdenum-bearing minerals react with oxygen and water, they produce molybdate ion is less soluble. Acute exposure to elevated molybdenum levels causes adverse health effects such as diarrhea, anemia, and gout; while chronic exposure causes weakness, fatigue, lack of appetite, anorexia, liver dysfunction, joint pain, osteoporosis, Cu deficiencies and pneumoconiosis (WHO, 2011a, b). Molybdenum is an important alloying agent, which strengthens the steel and decreases its weight (Henckens et al., 2018). A potential source of molybdenum in Qatar's GW could be from the oil and gas-processing sector as mainly the local natural gas is a sulfur containing as molybdenum is used as a catalyst in the desulfurization process (Kuiper et al., 2015). According to the international molybdenum association, molybdenum is also used in the manufacturing of pigments, corrosion inhibitors, smoke suppressants, lubricants, and fertilizer (IMOA, 2018).

Lithium levels in 39 samples exceeded the GSO and Qatar (KAHRAMAA) requirements for the water quality distribution systems in Qatar. Lithium is a naturally occurring alkali metal with an atomic number of three, it is found in many igneous rocks and several natural brines (Weil and Ziemann, 2014). The main sources of lithium are lithium-containing wastes such as produced petroleum water (Isupov et al., 1999). Lithium is alkali metal that is characterized by high electrochemical activity due to the quick loss of electrons; thus, lithium is a significant producer of electric current (Wang et al., 2016).

Strontium in 40 samples exceeded the US-EPA lifetime health advisory, the GSO, and the Qatar drinking water guidelines. Strontium commonly occurs in nature. It is primarily used in television cathode ray tubes. Strontium is used in glow in the dark toys, red firework and strontium chloride is used in toothpastes for sensitive teeth. Strontium in the human body is absorbed like it the lighter congener calcium due to

the chemical similarity. In children, strontium can substitute calcium and thus lead to bone growth issues. Uranium levels in one sample exceeded the WHO, GSO, and Qatar drinking water guidelines and one sample exceeded the US-EPA drinking water guidelines. Boron levels in 39 samples exceeded the USEPA guidelines for short-term use of irrigation water, 20 exceeded the USEPA guidelines for long-term use of irrigation water and three samples exceeded the Qatar irrigation guidelines. Molybdenum levels in 40 samples exceeded the USEPA guidelines for short-term use of irrigation water, 18 exceeded USEPA guidelines for long-term use of irrigation water. Selenium levels in one sample exceeded the US-EPA irrigation guidelines. Chromium levels in two samples exceeded the Qatar irrigation guidelines.

4. Conclusion

The GW in Qatar is mainly used for agricultural use. The significant increases of the population and agricultural activities have driven to the high extraction of the GW that negatively impacts its quantity and quality. Salinity is the most GW quality concern. The high salinity of the analyzed samples may be the result of climate conditions of high temperature and low rainfall, high evaporation, increasing agricultural activities, and the intrusion of brackish water from deep aquifers or with seawater intrusion. Most exceedances of the drinking water standards pertained to aesthetic qualities rather than health-based concerns. The results showed that $Na^+ > Ca^{2+} > Mg^{2+} > K^+$ was the sequence of major cations and $Cl^- > SO_4^{2-} > HCO_3^- > NO_3^-$ is the order of the main anions. The hydrogeochemical facies and Piper plots further confirmed that most of the analyzed GW samples were falling in the field of SO_4–Cl and Ca–Mg (permanent hardness); calcium chloride type and SO_4–Cl and Na–K (saline); sodium-chloride-type of water type indicating the permanent (non-carbonate) hardness in the majority of the analyzed samples. This result suggests halite dissolution, ion exchange, and seawater mixing. The GW hydrochemistry results revealed high levels of nitrate might be due to the agricultural activities and leakage of unrehabilitated sewage systems. Based on the geochemical PHREEQC modeling results, the chemical equilibrium and saturation indices showed oversaturation of calcite, dolomite, while anhydrite, gypsum, and halite show under-saturation. Principal component analysis reveals three main components that explain >99% of the total variance. The result showed the dissolution of evaporite minerals halite and gypsum, localized sedimentary depositional or hydrogeochemical environment, irrigation return flows, and nitrate fertilizers. The results showed that most of the analyzed anions and cations quality parameters in the GW are higher than the regional and international guidelines for the drinking water. The irrigation hazard analysis indicates that 60.9% of the GW samples, with specific electrical conductivity greater than 5000 μS/cm, would likely cause harm to agriculture, and only salt-tolerant crops are suitable. The 34% of the irrigation water was C4S2 and C4S3 of very high salinity hazard and medium sodium hazard, and very high salinity hazard and high sodium hazard respectively, indicating that the irrigation hazard is always higher from salinity than from SAR, thus it is not suitable for irrigation in almost all soils, except soils with high permeability.

This study assists managers and decision-makers to manage the GW and improve water quality used for irrigation. The obtained results illustrated that 95% of the GW was just suitable for irrigation certain tolerable crops in high permeability soil. Therefore, the following recommendations should be implemented according to the results of this study. Salinity reduction could be achieved by mixing saline water with low salinity water. The mixing process was already conducted by the national water supplier as they mix GW with treated wastewaters. The development of a low-cost treatment technique that can efficiently and simultaneously remove undesirable elements in the GW is highly recommended. This will help to enhance water security at the national level to yield a GW with superior quality and quantity. Additionally, the GW managers should supervise and optimize the quantity of irrigation water to prevent further deterioration of the GW quality. The current irrigation practices use flood irrigation, which enhances evaporation and thus increase the salt level in soil that could be leached to the GW. Thus, the farmer's awareness on the importance of the GW conservation should be increased. Farmers should be encouraged to use alternative agricultural practices such as using modern irrigation techniques like drip and sprinkler irrigation, use salt-tolerant and low water demand crops, and reduce the application of chemical fertilizers and pesticides.

Declaration of competing interest

The authors declare that they have no known competing financial interests or personal relationships that could have appeared to influence the work reported in this paper.

Acknowledgment

This publication was made possible by NPRP grant # [12S-0307–190250] from the Qatar National Research Fund (a member of Qatar Foundation). The findings achieved herein are solely the responsibility of the author[s]. The authors would like to thank the Central Laboratory Unit at Qatar University for their great assistance in analyzing the metal content in the groundwater samples.

Appendix A. Supplementary data

Supplementary data to this article can be found online at https://doi.org/10.1016/j.gsd.2020.100467.

References

Abdel-Satar, A.M., Al-Khabbas, M.H., Alahmad, W.R., Yousef, W.M., Alsomadi, R.H., Iqbal, T., 2017. Quality assessment of groundwater and agricultural soil in Hail region, Saudi Arabia. Egypt. J. Aquat. Res. 43 (1), 55–64. https://doi.org/10.1016/j.ejar.2016.12.004.

Adimalla, N., Venkatayogi, S., 2018. Geochemical characterization and evaluation of groundwater suitability for domestic and agricultural utility in semi-arid region of Basara, Telangana State, South India. Appl. Water Sci. 8 (1) https://doi.org/10.1007/s13201-018-0682-1.

Al-Farraj, A.S., Al-Wabel, M.I., El-Saeid, M.H., El-Naggar, A.H., Ahmed, Z., 2013. Evaluation of groundwater for arsenic contamination using hydrogeochemical properties and multivariate statistical methods in Saudi Arabia. J. Chem. 2013, 1–9. https://doi.org/10.1155/2013/812365.

Alfy, M.E., Lashin, A., Abdalla, F., Al-Bassam, A., 2017. Assessing the hydrogeochemical processes affecting groundwater pollution in arid areas using an integration of geochemical equilibrium and multivariate statistical techniques. Environ. Pollut. 229, 760–770. https://doi.org/10.1016/j.envpol.2017.05.052.

Al-Ghouti, M.A., Disi, Z.A.A., Al-Kaabi, N., Khraisheh, M., 2017. Mechanistic insights into the remediation of bromide ions from desalinated water using roasted date pits. Chem. Eng. J. 308, 463–475. https://doi.org/10.1016/j.cej.2016.09.091.

Al-Kalbani, M.S., Price, M.F., 2015. Sustainableaflajwater management in Al jabal Al akhdar, sultanate of Oman. Water Resour. Manag. VIII https://doi.org/10.2495/wrm150031.

Al-Naimi, L.S., Mgbeojedo, T.I., 2018. Hydrogeochemical evaluation of groundwater in parts of shamal, northern Qatar. Environ. Manag. Sustain. Dev. 7 (2), 181. https://doi.org/10.5296/emsd.v7i2.13046.

Al-Saad, H., 2005. Lithostratigraphy of the Middle Eocene Dammam formation in Qatar, arabian Gulf: effects of sea-level fluctuations along a tidal environment. J. Asian Earth Sci. 25 (5), 781–789. https://doi.org/10.1016/j.jseaes.2004.07.009.

Alsharhan, A.S., Rizk, Z.A., Nairn, A.E.M., Bakhit, D.W., Alhajari, S.A., 2001. Hydrogeology of an Arid Region: the Arabian Gulf and Adjoining Areas, vol. 2001. Elsevier.

Al-Shidi, F.K., 2014. Study the Quality of Groundwater of Al-Zoroup Area in Mahdah State, the Sultanate of Oman. United Arab Emirates University. https://scholarworks.uaeu.ac.ae/all_theses/12.

Alsuhaimi, A.O., Almohaimidi, K.M., Momani, K.A., 2019. Preliminary assessment for physicochemical quality parameters of groundwater in Oqdus Area, Saudi Arabia. J. Saudi Soc. Agric. Sci. 18 (1), 22–31. https://doi.org/10.1016/j.jssas.2016.12.002.

Al-Yousef, M., 2003. Mineralogy, Geochemistry and Origin of Quaternary Sabkhas in the Qatar Peninsula, Arabian Gulf. PhD Thesis. University of Southampton, p. 437.

Baalousha, H.M., Weber, T., McPhee, M.J., Anderssen, 2015. Estimation of natural groundwater recharge in Qatar using GIS. MODSIM2015. In: 21st International Congress on Modelling and Simulation. https://doi.org/10.36334/modsim.2015.l2.baalousha.

Baalousha, H.M., 2016. Groundwater vulnerability mapping of Qatar aquifers. J. Afr. Earth Sci. 124, 75–93. https://doi.org/10.1016/j.jafrearsci.2016.09.017.

Czerewko, M., Cripps, J., Reid, J., Duffell, C., 2003. Sulfur species in geological materials—sources and quantification. Cement Concr. Compos. 25 (7), 657–671. https://doi.org/10.1016/s0958-9465(02)00066-5.
El gawad, E.A.A., Lotfy, M.M., Sadooni, F.N., Katheery, B., 2008. Assessment of the oil pollution extent in the offshore sediments, Abu Dhabi, UAE. Austral. J. Basic Appl. Sci. 2 (3), 561–574.
El Maghraby, M.M.S., El Nasr, A.K.O.A., Hamouda, M.S.A., 2013. Quality assessment of groundwater at south Al Madinah Al Munawarah area, Saudi Arabia. Environ. Earth Sci. 70 (4), 1525–1538.
Etteieb, S., Cherif, S., Tarhouni, J., 2015. Hydrochemical assessment of water quality for irrigation: a case study of the Medjerda River in Tunisia. Appl. Water Sci. 7 (1), 469–480. https://doi.org/10.1007/s13201-015-0265-3.
FAO, 1994. Water Quality for Agriculture. Food and Agriculture Organization, Irrigation and Drainage Papers. ISBN 92-5-102263-1. Retrieved from. http://www.fao.org/docrep/003/t0234e/t0234e00.htm.
Galitskaya, I., Kostikova, I., Pozdnyakova, I., Zhigalin, A., 2013. The role of rock in chemical and isotopic composition of groundwater in the vicinity of radioactive waste disposal site. Procedia Earth Planet. Sci. 7, 276–279. https://doi.org/10.1016/j.proeps.2013.03.072.
Ghalib, H.B., 2017. Groundwater chemistry evaluation for drinking and irrigation utilities in east Wasit province, Central Iraq. Appl. Water Sci. 7 (7), 3447–3467. https://doi.org/10.1007/s13201-017-0575-8.
GSO, GCC Standardization Organization, 2008. Unbottled Drinking Water Standard. Retrieved from. https://www.gso.org.sa/en/.
Hasenmueller, E.A., Criss, R.E., 2013. Multiple sources of boron in urban surface waters and groundwaters. Sci. Total Environ. 447, 235–247. https://doi.org/10.1016/j.scitotenv.2013.01.001.
Henckens, M., Driessen, P., Worrell, E., 2018. Molybdenum resources: their depletion and safeguarding for future generations. Resour. Conserv. Recycl. 134, 61–69. https://doi.org/10.1016/j.resconrec.2018.03.002.
Hoyos, I.P., Krakauer, N., Khanbilvardi, R., Armstrong, R., 2016. A review of advances in the identification and characterization of groundwater dependent ecosystems using geospatial technologies. Geosciences 6 (2), 17. https://doi.org/10.3390/geosciences6020017.
IMOA, 2018. Annual Review 2018/2019. International Molybdenum Association. Retrieved from. https://www.imoa.info/molybdenum-media-centre/downloads/annual-review.php.
ISO 5667-11:2009, 2009. Water Quality Sampling, Part 11. Retrieved from. https://www.iso.org/standard/42990.html.
Isupov, V., Kotsupalo, N., Nemudry, A., Menzeres, L., 1999. Aluminium hydroxide as selective sorbent of lithium salts from brines and technical solutions. In: Studies in Surface Science and Catalysis Adsorption and its Applications in Industry and Environmental Protection, vol. I. Applications in Industry, pp. 621–652. https://doi.org/10.1016/s0167-2991(99)80567-9.
Jolliffe, I.T., Cadima, J., 2016. Principal component analysis: a review and recent developments. Phil. Trans. Math. Phys. Eng. Sci. 374 (2065), 20150202. https://doi.org/10.1098/rsta.2015.0202.
Khan, Q., Kalbus, E., Alshamsi, D.M., Mohamed, M.M., Liaqat, M.U., 2019. Hydrochemical analysis of groundwater in remah and Al khatim regions, United Arab Emirates. Hydrology 6 (3), 60. https://doi.org/10.3390/hydrology6030060.
Kuiper, N., Rowell, C., Shomar, B., 2015. High levels of molybdenum in Qatar's groundwater and potential impacts. J. Geochem. Explor. 150, 16–24. https://doi.org/10.1016/j.gexplo.2014.12.009.
Kumar, S.K., Rammohan, V., Sahayam, J.D., Jeevanandam, M., 2009. Assessment of groundwater quality and hydrogeochemistry of Manimuktha River basin, Tamil Nadu, India. Environ. Monit. Assess. 159, 341–351.
Machado, R., Serralheiro, R., 2017. Soil salinity: effect on vegetable crop growth. Management practices to prevent and mitigate soil salinization. Horticulturae 3 (2), 30. https://doi.org/10.3390/horticulturae3020030.
Mallick, J., Singh, C., Almesfer, M., Kumar, A., Khan, R., Islam, S., Rahman, A., 2018. Hydro-geochemical assessment of groundwater quality in aseer region, Saudi Arabia. Water 10 (12), 1847. https://doi.org/10.3390/w10121847.
Manickum, T., John, W., Terry, S., Hodgson, K., 2014. Preliminary study on the radiological and physicochemical quality of the Umgeni Water catchments and drinking water sources in KwaZulu-Natal, South Africa. J. Environ. Radioact. 137, 227–240. https://doi.org/10.1016/j.jenvrad.2014.07.015.
Marghade, D., Malpe, D.B., Zade, A.B., 2011. Geochemical characterization of groundwater from northeastern part of Nagpur urban, Central India. Environ. Earth Sci. 62 (7), 1419–1430.
MDPS, Ministry of Development Planning and Statistics, 2015. Water Statistics in the State of Qatar 2015. Retrieved November 18, 2017, from. https://www.mdps.gov.qa/en/statistics1/pages/topicslisting.aspx?parent=Environmental&child=Water.
MDPS, Ministry of Development Planning and Statistics, 2018. Population Statistics in the State of Qatar 2018. Retrieved May 1, 2018, from. https://www.mdps.gov.qa/ar/statistics1/pages/topicslisting.aspx?parent=Population&child=Population.
Misstear, B., Banks, D., Clark, L., 2017. Water Wells and Boreholes. https://doi.org/10.1002/9781119080176.
Mohammad, R. Jafari, Francois, G. Bernardeau, 2019. Deep injection wells for flood prevention and groundwater management. Int. Scholar. Sci. Res. Innov. 13 (5), 2019, ISNI:0000000091950263, World Academy of Science, Engineering and Technology International Journal of Geotechnical and Geological Engineering Vol: 13, No:5, 2019.
Othman, A.K., 2005. Quantitative and Qualitative Assessment of Groundwater Resources in Al-Khatim Area (Uae).
Rajmohan, N., Niazi, B.A.M., Masoud, M.H.Z., 2019. Evaluation of a brackish groundwater resource in the Wadi Al-Lusub basin, Western Saudi Arabia. Environ. Earth Sci. 78 (15) https://doi.org/10.1007/s12665-019-8441-7.
Ravikumar, P., Somashekar, R.K., 2015. Principal component analysis and hydrochemical facies characterization to evaluate groundwater quality in Varahi river basin, Karnataka state, India. Appl. Water Sci. 7 (2), 745–755. https://doi.org/10.1007/s13201-015-0287-x.
Sadiq, A.M., Nasir, S.J., 2002. Middle pleistocene karst evolution in the state of Qatar, arabian Gulf. J. Cave Karst Stud. 64 (2), 132–139.
Seyedmohammadi, J., Esmaeelnejad, L., Shabanpour, M., 2016. Spatial variation modelling of groundwater electrical conductivity using geostatistics and GIS. Model. Earth Syst. Environ. https://doi.org/10.1007/s40808-016-0226-3.
Srinivasamoorthy, K., Gopinath, M., Chidambaram, S., Vasanthavigar, M., Sarma, V.S., 2014. Hydrochemical characterization and quality appraisal of groundwater from Pungar sub basin, Tamilnadu, India. J. King Saud Univ. Sci. 26 (1), 37–52.
Sundaram, B., Feitz, A.J., de Caritat, P., Plazinska, A., Brodie, R.S., Coram, J., Australia, G., 2009. Groundwater Sampling and Analysis: A Field Guide. Geoscience Australia. Retrieved from. http://ga.gov.au/image_cache/GA15501.pdf.
SWS, Schlumberger Water Services, 2009. Studying and Developing the Natural and Artificial Recharge of the Groundwater in Aquifer in the State of Qatar. Department of Agriculture and Water Research (DAWR), Ministry of Environment, State of Qatar.
Shamrukh, M., 2012. Exploring of Deep Groundwater in the Southwest Aquifer of Qatar. Department of Water, Ministry of Environment, P.O. Box 7634, Doha, Qatar. https://doi.org/10.13140/2.1.3191.5521.
Sherif, M., Mohamed, M., Kacimov, A., Shetty, A., 2011. Assessment of groundwater quality in the northeastern coastal area of UAE as precursor for desalination. Desalination 273 (2–3), 436–446. https://doi.org/10.1016/j.desal.2011.01.069.
Shomar, B., Darwish, M., Rowell, C., 2014. What does integrated water resources management from local to global perspective mean? Qatar as a case study, the very rich country with No water. Water Resour. Manag. 28 (10), 2781–2791. https://doi.org/10.1007/s11269-014-0636-9.
Shomar, B., 2015. Geochemistry of soil and groundwater in arid regions: Qatar as a case study. Groundwater Sustain. Develop. 1 (1–2), 33–40. https://doi.org/10.1016/j.gsd.2015.12.005.
Smedley, P.L., Kinniburgh, D.G., 2017. Molybdenum in natural waters: a review of occurrence, distributions and controls. Appl. Geochem. 84, 387–432. https://doi.org/10.1016/j.apgeochem.2017.05.008.
Suursoo, S., Hill, L., Raidla, V., Kiisk, M., Jantsikene, A., Nilb, N., Isakar, K., 2017. Temporal changes in radiological and chemical composition of Cambrian-Vendian groundwater in conditions of intensive water consumption. Sci. Total Environ. 601–602, 679–690. https://doi.org/10.1016/j.scitotenv.2017.05.136.
UNDP, United Nations Development Programme, 2013. Water Governance in the Arab Region: Managing Scarcity and Securing the Future (New York, NY).
USDA, 2000. Heavy Metal Soil Contamination. Natural Resources Conservation Service. United States Department of Agriculture. Retrieved from. https://www.nrcs.usda.gov/Internet/FSE_DOCUMENTS/nrcs142p2_053279.pdf.
Vengosh, A., Gill, J., Lee Davisson, M., Bryant Hudson, G., 2002. A multi-isotope (B, Sr, O, H, and C) and age dating (3H–3He and 14C) study of groundwater from Salinas Valley, California: hydrochemistry, dynamics, and contamination processes. Water Resour. Res. 38 (1), 9–1.
Vinson, D.S., Tagma, T., Bouchaou, L., Dwyer, G.S., Warner, N.R., Vengosh, A., 2013. Occurrence and mobilization of radium in fresh to saline coastal groundwater inferred from geochemical and isotopic tracers (Sr, S, O, H, Ra, Rn). Appl. Geochem. 38, 161–175. https://doi.org/10.1016/j.apgeochem.2013.09.004.
Voutsa, D., Dotsika, E., Kouras, A., Poutoukis, D., Kouimtzis, T., 2009. Study on distribution and origin of boron in groundwater in the area of Chalkidiki, Northern Greece by employing chemical and isotopic tracers. J. Hazard Mater. 172 (2–3), 1264–1272. https://doi.org/10.1016/j.jhazmat.2009.07.132.
Walsh, M., Wallner, G., Jennings, P., 2014. Radioactivity in drinking water supplies in Western Australia. J. Environ. Radioact. 130, 56–62. https://doi.org/10.1016/j.jenvrad.2013.12.016.
Wang, F., Wu, X., Li, C., Zhu, Y., Fu, L., Wu, Y., Liu, X., 2016. Nanostructured positive electrode materials for post-lithium ion batteries. Energy Environ. Sci. 9 (12), 3570–3611. https://doi.org/10.1039/c6ee02070d.
Weil, M., Ziemann, S., 2014. Recycling of traction batteries as a challenge and chance for future lithium availability. Lithium-Ion Batteries 509–528. https://doi.org/10.1016/b978-0-444-59513-3.00022-4.
WHO, 2011a. Guidelines for Drinking-Water Quality, fourth ed. World Health Organization, Geneva. Retrieved from. https://www.who.int/water_sanitation_health/publications/dwq-guidelines-4/en/.
WHO, 2011b. Molybdenum in Drinking Water: Background Document for Devel- Opment of WHO Guidelines for Drinking-Water Quality (WHO/SDE/WSH/03.04/11/Rev/1. World Health Organization, Geneva, Switzerland.
Guidelines for drinking-water quality: fourth edition incorporating the first addendum. Geneva: World Health Organization; 2017. Licence: CC BY-NC-SA 3.0 IGO. Retrieved from https://www.who.int/water_sanitation_health/publications/drinking-water-quality-guidelines-4-including-1st-addendum/en/.